

ORIGINAL ARTICLE OPEN ACCESS

The Role of Dietary Polyphenols in the Prevention of Non-Communicable Chronic Diseases

Polygonati Rhizoma Attenuates Oxidative Stress-Induced Senescence in Periodontal Ligament Stem Cells

Xinran Feng¹  | Ying An¹ | Fanfan Hou¹ | Qian Guo^{2,3}  | Shanshan Cai⁴  | Hongbin Xu⁵  | Youfu He⁶ 

¹State Key Laboratory of Oral & Maxillofacial Reconstruction and Regeneration, National Clinical Research Center for Oral Diseases, Shaanxi International Joint Research Center for Oral Diseases, The Second Medical Center, School of Stomatology, The Fourth Military Medical University, Xi'an, China | ²Department of Respiratory and Critical Care Medicine, The First Affiliated Hospital of Zhengzhou University, Zhengzhou, China | ³Department of Rhinology, First Affiliated Hospital of Zhengzhou University, Zhengzhou, China | ⁴Division of Biomedical and Life Sciences, Faculty of Health and Medicine, Lancaster University, Lancaster, UK | ⁵Longhua Hospital, Shanghai University of Traditional Chinese Medicine, Shanghai, China | ⁶Department of Cardiology, Guizhou Provincial People's Hospital, Guiyang, Guizhou Province, China

Correspondence: Hongbin Xu (hongbinxu@126.com) | Qian Guo (guoqianmail@163.com) | Shanshan Cai (s.cai6@lancaster.ac.uk) | Youfu He (heyufu0912@163.com)

Received: 23 November 2025 | **Revised:** 25 February 2026 | **Accepted:** 10 March 2026

Keywords: dentistry | network pharmacology | periodontal ligament stem cells | periodontitis | periodontology | *Polygonati Rhizoma*

ABSTRACT

Periodontitis is increasingly recognized as a non-communicable chronic oral disease in which sustained oxidative stress and cellular senescence drive low-grade inflammation and tissue destruction. *Polygonati Rhizoma* (*PR*), a traditional Chinese herb widely consumed as a functional food ingredient, is rich in antioxidant polyphenols and polysaccharides, yet its role in modulating senescence of periodontal ligament stem cells (PDLSCs) remains unclear. This study integrated network pharmacology and experimental validation to elucidate the protective effects and mechanisms of *PR* against oxidative stress-induced PDLSC senescence. Putative *PR* components and targets related to periodontitis and aging were collected to construct a protein–protein interaction (PPI) network, from which 21 core targets were predicted. These included key inflammation- and senescence-related proteins such as TP53, RELA (p65), TNF- α , TGF- β 1, IL-6, IL-1 β , CXCL8, and MMP-9. Gene Ontology and KEGG enrichment analyses highlighted pathways involved in cellular senescence, NF- κ B signaling, and oxidative stress responses. Molecular docking suggested strong binding affinities between major *PR* constituents and putative core protein targets. In an in vitro oxidative stress-induced PDLSC senescence model, *PR*-medicated serum, with Metformin as a positive control, significantly reduced intracellular oxidative stress markers, alleviated cell-cycle arrest, and downregulated senescence-associated secretory phenotype (SASP) cytokines. *PR* showed anti-senescent efficacy comparable to Metformin while exhibiting distinct molecular signatures. These findings indicate that *PR* exerts multi-component, multi-target modulation of NF- κ B-centered inflammatory and senescence pathways in PDLSCs, thereby mitigating oxidative stress-induced cellular aging. As an edible, functional herb, *PR* may represent a promising dietary adjunct for the prevention and management of periodontitis linked to cellular senescence.

1 | Introduction

Periodontitis is the primary cause of tooth loss in adults and is characterized by chronic infection that results in the progressive loss of epithelial attachment and alveolar bone (Papapanou et al. 2018). The global prevalence of periodontitis is estimated

between 20% and 50% (Czesnikiewicz-Guzik et al. 2019). In 2010, severe periodontitis was the 6th most prevalent condition, affecting approximately 743 million people worldwide; a figure that surged to 1.1 billion cases by 2019 (Global, Regional, and National Incidence, Prevalence, and Years Lived With Disability for 354 Diseases and Injuries for 195 Countries and

This is an open access article under the terms of the [Creative Commons Attribution](https://creativecommons.org/licenses/by/4.0/) License, which permits use, distribution and reproduction in any medium, provided the original work is properly cited.

© 2026 The Author(s). *Food Science & Nutrition* published by Wiley Periodicals LLC.

Territories, 1990–2017: A Systematic Analysis for the Global Burden of Disease Study 2017 (2018). Conventional treatments primarily aim to control plaque and reduce inflammation, but often fail to restore damaged periodontal tissues fully, leading to inconsistent clinical outcomes (Meng et al. 2022; Sanz et al. 2020). Advances in regenerative medicine, particularly tissue engineering, now offer promising prospects for periodontal regeneration using mesenchymal stem cells (MSCs) (Iwayama et al. 2022; Nguyen-Thi et al. 2023). Among these, periodontal ligament stem cells (PDLSCs) stand out for their exceptional ability to form cementum and periodontal ligament-like structures (Nguyen-Thi et al. 2023; Wen et al. 2024). However, despite progress in cell isolation techniques (Behfarnia et al. 2023; Rad et al. 2022), maintaining cell viability remains a challenge due to issues like cellular senescence and inflammation, which impede the effectiveness of tissue engineering (Lin et al. 2024). As a result, optimizing the use of PDLSCs for periodontal regeneration remains a key focus for ongoing and future research.

Periodontitis is a chronic, multifactorial disease triggered by a dysbiotic biofilm and sustained by an aberrant host response (Kinane et al. 2017). Although chronological aging per se is not an independent risk factor for periodontitis, does not clearly alter plaque microbiology, and has only a limited impact on treatment response (Needleman and Clark 2023), multiple hallmarks of biological aging—notably cellular senescence, stem, progenitor cell exhaustion, and immune-senescence—are increasingly documented in periodontal tissues and are mechanistically linked to disease susceptibility and progression (Aquino-Martinez 2023; Baima et al. 2022). Mechanistically, as the first line of defense against bacterial invasion, polymorphonuclear neutrophils (PMNs) undergo a respiratory burst during phagocytosis, releasing large amounts of reactive oxygen species (ROS) that induce oxidative stress, thereby damaging DNA, lipids, and proteins and accelerating cellular senescence (Liguori et al. 2018; Maldonado et al. 2023; Nouis et al. 2023). Senescent cells secrete factors characteristic of the senescence-associated secretory phenotype (SASP)—including pro-inflammatory cytokines, chemokines, growth factors, and matrix metalloproteinases (MMPs)—which amplify inflammation and disrupt tissue homeostasis (Aquino-Martinez 2023; Baima et al. 2022). In parallel, cellular senescence and chronic inflammation can drive stem cell exhaustion, reducing stem cell number and function and impairing MSCs' self-renewal, multilineage differentiation, and immunomodulatory capacity, thereby hindering periodontal healing and regeneration (Aquino-Martinez 2023; Baima et al. 2022; Cai et al. 2022; López-Otín et al. 2023). Against this background, PDLSCs are considered ideal candidates for periodontal regeneration (Shang et al. 2017); delineating their aging process not only clarifies the intersection between periodontitis and biological aging but may also reveal new therapeutic targets.

Polygonati Rhizoma (PR) was first documented in *Shen Nong's Herbal Classic* during the Eastern Han Dynasty (25–220 AD). It refers to the dried rhizome of *Polygonatum kingianum* Col. et Hemsl., *Polygonatum sibiricum* Red., or *Polygonatum cytonema* Hua, as described in the Chinese Pharmacopoeia (2020 edition) (National Pharmacopoeia 2020). Modern pharmacological and medicinal chemistry studies have identified various bioactive compounds in *PR*, including polysaccharides, steroidal

saponins, triterpenes, alkaloids, lignans, flavonoids, and phytosterols. These compounds exhibit anti-aging effects through multiple mechanisms, such as anti-inflammatory, antioxidant, immunoregulatory, mitochondrial protection, and telomerase activation (Zhao et al. 2023). However, the specific biomarkers and biological pathways by which the active components of *PR* mitigate the senescence of PDLSCs remain unclear. Therefore, this study aims to evaluate the potential anti-senescence effects of *PR* active components on oxidative stress-induced PDLSCs and to elucidate the underlying molecular mechanisms. To this end, we tested the null hypothesis (H_0) that *PR* active components exert no protective effect on the senescence of PDLSCs under oxidative stress.

2 | Materials and Methods

This investigation combines network pharmacology with experimental validation to elucidate the anti-aging mechanisms of *PR* against oxidative-stress-induced PDLSC in senescence. A schematic overview of the study workflow is presented in Figure 1.

2.1 | Network Pharmacology Analysis

2.1.1 | Identification of Active Ingredients and Potential Targets of *PR*

The chemical composition of *PR* was obtained from several databases, including Traditional Chinese Medicine Systems Pharmacology Database and Analysis Platform (TCMSP) (Ru et al. 2014), Traditional Chinese Medicine Information Database (TCM-ID) (Chen et al. 2006), Herbal Ingredients' Targets Platform (HIT) (Ye et al. 2011), The Encyclopedia of Traditional Chinese Medicine (ETCM) (Xu et al. 2019), and Traditional Chinese Medicine Database@Taiwan (TCM Database@Taiwan) (Chen 2011). Active ingredients were identified based on the criteria of oral bioavailability (OB) $\geq 30\%$ and drug-likeness (DL) ≥ 0.18 . Additionally, components that did not meet these criteria but were reported in the literature as active ingredients, quality markers, or compounds with anti-aging properties or efficacy in treating periodontitis were also included. The active ingredients were then subjected to target prediction using the TCMSP, HIT, SwissTargetPrediction (Daina et al. 2019), and Similarity ensemble approach (SEA) (Keiser et al. 2007) databases. Predicted targets were cross-referenced with the UniProtKB database (UniProt Consortium 2021) for protein name annotation and corresponding gene symbol identification.

2.1.2 | Selection of Aging-Related Targets of PDLSCs

The GeneCards (Stelzer et al. 2016), Disease Gene Network (DisGeNET) (Piñero et al. 2020), Therapeutic Target Database (TTD) (Zhou et al. 2022), DrugBank database (Wishart et al. 2018), and ETCM databases were queried using the keyword “periodontitis” to identify targets associated with the condition. Furthermore, specialized aging databases, including Aging Atlas (AgingAtlas Consortium 2021), GenAge (Tacutu et al. 2018), and Open Genes (Rafikova et al. 2024), were searched to identify aging-related targets. By intersecting these

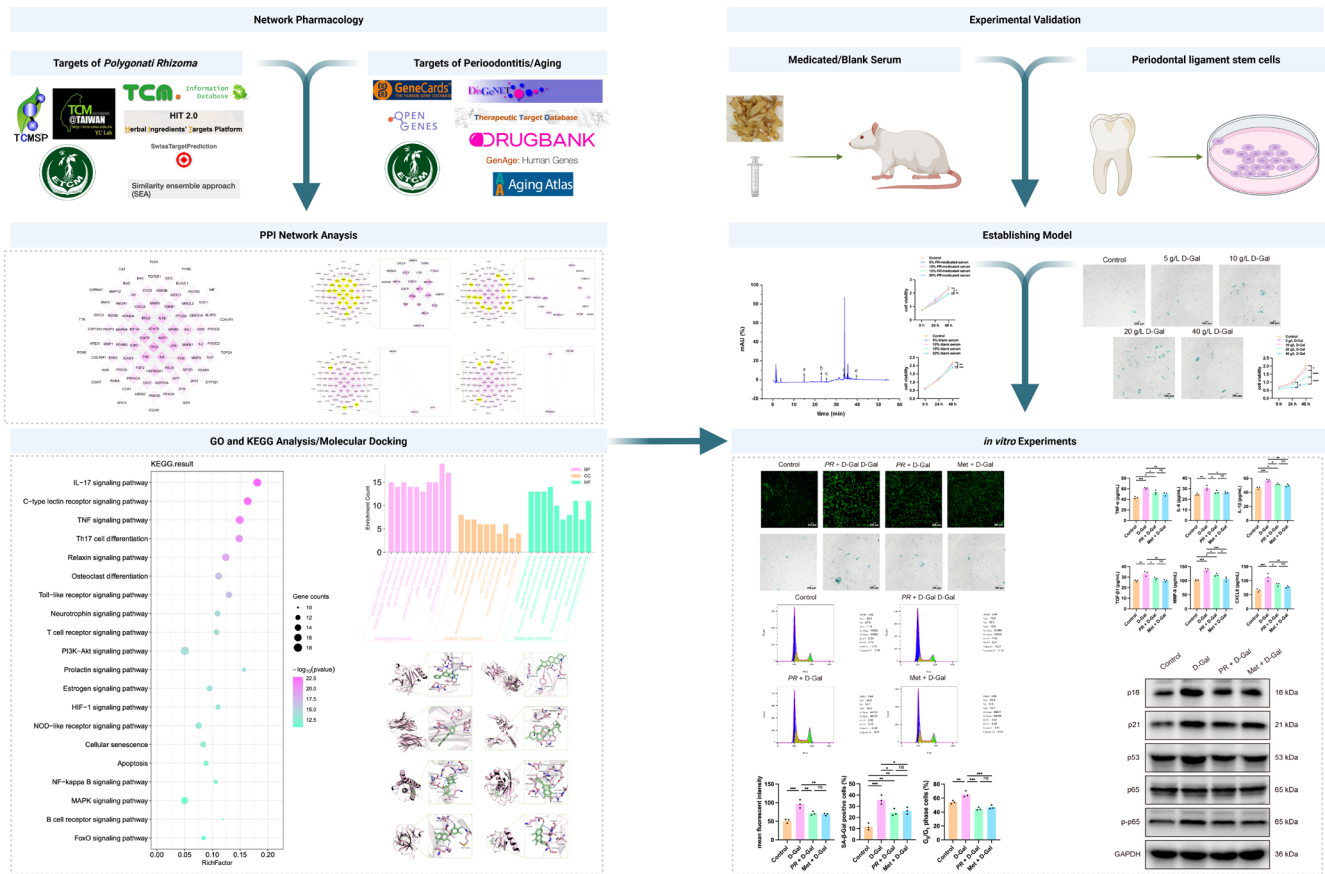


FIGURE 1 | Study methodology flowchart.

two target sets, we identified aging-related targets relevant to PDLSCs.

2.1.3 | Construction of Protein and Protein Interaction (PPI) Network and Enrichment Analysis

The PPI network was constructed using the Search Tool for Retrieval of Interacting Genes/Proteins (STRING) database (Szklarczyk et al. 2021), employing the “Multiple proteins” function, with the species restricted to “*Homo sapiens*”, and the minimum required interaction score set to “high confidence (0.700)”. The resulting PPI network was then imported into *CytoScape* 3.10.1 software for visualization. The degree centrality (DC), closeness centrality (CC), and betweenness centrality (BC) of network nodes were calculated using the *cytoHubba* plugin. The Molecular Complex Detection (MCODE) plugin (Bader and Hogue 2003) was then used to cluster the network and identify core sub-networks and key targets. Gene Ontology (GO) (GeneOntologyConsortium 2015) and Kyoto Encyclopedia of Genes and Genomes (KEGG) (Ogata et al. 1999) enrichment analyses of the key targets were conducted using the *clusterProfiler* package in R 4.3.2 software.

2.1.4 | Molecular Docking

Protein crystal structures were retrieved from the Research Collaboratory for Structural Bioinformatics Protein Data Bank

(RCSB PDB) database (Berman et al. 2000). *PyMOL* open-source software version 4.6.0 was used to remove water molecules and redundant protein chains. Original ligands were separated to define the center and dimensions of the docking box. The processed structures were then converted to “Protein Data Bank, Partial Charge & Atom Type” (PDBQT) format using *AutoDockTool* (Morris et al. 2009) software version 1.5.7.

The 3D structure of small molecules was obtained from the PubChem database in “Structure-Data File (SDF)” format and converted to “PDBQT” format using *OpenBabel* (O’Boyle et al. 2011) software version 3.1.1. This conversion involved adding polar hydrogens, assigning charges according to the Merck Molecular Force Field, 1994 parameter set (MMFF94) force field, and performing energy minimization. The active components of *PR* were docked with the core targets using *AutoDock Vina* software version 1.1.2. Interaction patterns were analyzed using Protein-Ligand Interaction Profiler (*PLIP*) software version 2.2.0, and the results were visualized with *PyMol* open-source software version 4.6.0.

2.2 | Verification Experiments

2.2.1 | Cell Culture

The experiments involving human tissue samples were approved by the Ethics Committee of the School of Stomatology, China Medical University, Shenyang, China (K2023007). PDLSCs were

isolated and identified as described in our previous publications (Feng et al. 2024; Jing et al. 2024). Briefly, healthy premolars or third molars were collected from individuals aged 18–25 years at the university's dental clinic after informed consent. The extracted teeth were rinsed with 5% phosphate-buffered saline (PBS; Gibco, USA) containing 5% penicillin/streptomycin (PS; Gibco, USA) until blood stains were no longer visible. Periodontal tissues were then scraped from the middle third of the root, cut into small fragments, and distributed evenly into a 6-well plate containing 2 mL of low glucose-Dulbecco's Modified Eagle Medium (L-DMEM; Gibco, USA) supplemented with 20% fetal bovine serum (FBS; Gibco, USA) and 1% PS. The plates were incubated in a humidified atmosphere of 5% CO₂ at 37°C. The medium was replaced every three days until adherent cell outgrowth was observed under an inverted phase-contrast microscope (CKX31, OLYMPUS, Japan). Single-cell suspensions were prepared and diluted to 10 cells/mL, then plated into 96-well plates with 100 µL of L-DMEM containing with 10% FBS and 1% PS per well to cultivate individual clones. All monoclonal cell populations were pooled as passage 1 PDLSCs. Cells were sub-cultured approximately every three days at a 1:3 ratio upon reaching 80% confluence, with passages 3–5 used for subsequent experiments.

2.2.2 | Preparation of PR-Medicated Serum and Blank Serum

The animal experiments were approved by the Ethics Commission of China Medical University, Shenyang, China (Approval No. CMU20231000). Male Sprague–Dawley rats (8 weeks; 180–220 g) were purchased from SPF (Beijing) Biotechnology Co. Rats were housed under standard conditions (22°C–24°C; 60%–70% humidity; 12-h light–dark cycle) with free access to food and tap water. Twenty rats were randomly allocated (random-number table) to a control group and a high-dose PR group (20 g/kg). The PR group received once daily intragastric administration of PR, and the control group received physiological saline (1 mL/100 g), for 7 consecutive days.

On day 7 (2 h after the last administration), rats were anesthetized in an induction chamber with isoflurane (4%–5% for induction in 100% O₂ at 1.0 L/min) and maintained at 1.5%–2.5% isoflurane via a nose cone. Depth of anesthesia was confirmed by absence of pedal withdrawal and corneal reflexes. While under deep anesthesia, a midline laparotomy was performed, and blood was collected aseptically from the abdominal aorta using a sterile syringe; exsanguination under deep anesthesia served as the method of euthanasia, and bilateral thoracotomy was performed immediately thereafter to ensure death. Body temperature was maintained on a heating pad throughout the procedure. Serum was inactivated at 56°C for 30 min, sterile-filtered, and stored at –80°C until use.

2.2.3 | High Performance Liquid Chromatograph (HPLC)

To prepare the serum samples, 2 mL of each sample was mixed with 6 mL of methanol, vortexed for 10 min, and centrifuged at 18,000 rpm for 10 min at 4°C. The supernatant was collected,

evaporated under nitrogen, and reconstituted in 200 µL of 50% methanol. The solution was vortexed, sonicated for 10 min, and centrifuged again at 18,000 rpm for 10 min at 4°C. The supernatant was reserved for analysis.

To prepare the standard solutions, 2 mg each of β-sitosterol, bicalcain, kaempferol, myricetin, and diosgenin were accurately weighed and dissolved in 99.8% methanol (β-sitosterol was dissolved in DMSO) to create stock solutions at a concentration of 1 mg/mL. A 20 µL aliquot from each stock solution was combined into a single volumetric flask and diluted to 2 mL with 99.8% methanol (DMSO for β-sitosterol). This mixture was further diluted to prepare a mixed standard solution with a concentration of 10 µg/mL, then filtered through a 0.45 µm membrane for analysis.

Chromatographic separation was performed using an Agilent Poroshell 120 EC-C18 column (4.6 mm × 150 mm, 5 µm). The mobile phases were acetonitrile (phase A) and 0.1% phosphoric acid (phase B). Gradient elution was conducted as follows: 0–2 min at 90% B; 2–10 min decreasing to 80% B; 10–25 min decreasing to 65% B; 25–35 min decreasing to 5% B; 35–50 min at 5% B; 50–55 min returning to 90% B. The flow rate was 1.0 mL/min, with detection at 260 nm, a column temperature of 30°C, and an injection volume of 10 µL.

2.2.4 | Cell Viability

Cell viability was assessed using Cell Counting Kit-8 (CCK-8; APExBIO, USA) following the manufacturer's protocol. PDLSCs were seeded in 96-well plates at a density of 5 × 10³ per well and incubated in L-DMEM with 10% FBS at 37°C. After cell adhesion, the cells were treated with complete medium containing various concentrations of D-galactose (D-Gal; 5, 10, 20, and 40 g/L), PR-medicated serum (5%, 10%, 15%, and 20%), and blank serum (5%, 10%, 15%, and 20%). After 0, 24, and 48 h of stimulation, the medium was replaced with 90 µL of L-DMEM and 10 µL of CCK-8 solution per well. The plates were incubated at 37°C for 2 h. Absorbance was measured using a microplate reader (Tecan Mechelen, Belgium) at a test wavelength of 450 nm and a reference wavelength of 600 nm. Data were analyzed and plotted using *GraphPad Prism* (version 9.4.0).

2.2.5 | Cell Treatment

The following experiments were divided into four groups:

1. Control group: 24 h after plating, the cells were exposed to L-DMEM with 5% FBS, and 5% blank serum for 48 h.
2. D-Gal group: 24 h after plating, the cells were exposed to L-DMEM with 5% FBS, 5% blank serum, and 10 g/L D-Gal for 48 h.
3. PR + D-Gal group: 24 h after plating, the cells were exposed to L-DMEM with 5% FBS, 5% PR-medicated serum, and 10 g/L D-Gal for 48 h.
4. Met + D-Gal group: 24 h after plating, the cells were exposed to L-DMEM with 5% FBS, 5% blank serum, 10 g/L D-Gal, and 100 µM Met for 48 h.

2.2.6 | Intracellular Reactive Oxygen Species (ROS)

Intracellular ROS was detected using ROS Assay Kit (S0033S, Beyotime, China). According to the manufacturer's protocol, stimulated cells were washed with PBS and incubated in culture medium with 10 $\mu\text{mol/L}$ DCFH-DA at 37°C for 20 min. After incubation, the cells were washed three times with PBS and observed under an inverted phase-contrast microscope (OLYMPUS, Japan).

2.2.7 | Senescence-Associated β -Galactosidase (SA- β -Gal) Staining

SA- β -Gal staining was carried out with SA- β -Gal Staining Kit (Beyotime, China). Stimulated cells were washed with PBS, fixed with 4% paraformaldehyde for 15 min, and washed three times with PBS. The cells were then incubated with SA- β -Gal staining solution at 37°C without CO₂ overnight. Blue-stained cells were observed under an inverted phase-contrast microscope (OLYMPUS, Japan) and calculated using *ImageJ* software (version 1.8.0). The fraction of senescent cells was scored as the percentage of SA- β -Gal-positive cells relative to total cells.

2.2.8 | Cell Cycle

Cell cycle analysis was performed using Cell Cycle and Apoptosis Analysis Kit (C1052, Beyotime, China). After cell synchronization and treatment, PDLSCs were washed three times with cold PBS and fixed with 75% ethanol in PBS at -20°C for 12 h. The cells were then washed with cold PBS and stained with 0.5 mL of propidium iodide (PI) at 37°C for 30 min in the dark. Data were analyzed by flow cytometry (Becton Dickinson, USA) and *FlowJo* software (version 10.8.1).

2.2.9 | Enzyme-Linked Immunosorbent Assay (ELISA)

The SASP in the supernatants of stimulated cells was detected using ELISA Kits (Shanghai GuDuoBio Technology Co. Ltd., China). For this analysis, 50 μL of standards and samples, consisting of 10 μL of test samples and 40 μL of sample solution, were added to 96-well plates. The plates were sealed and incubated with 100 μL of Horseradish Peroxidase (HRP)-conjugated reagents per well at 37°C for 60 min. After five washes, 50 μL of substrates A and B were added to each well and incubated at 37°C for 15 min in the dark. Following the addition of 100 μL of stop solution, absorbance was measured at 450 nm using a microplate reader (Tecan Mechelen, Belgium). Standard curves and sample concentrations were calculated using linear regression in *Microsoft Excel* software (version 16.80).

2.2.10 | Western Blot

Total protein was extracted from stimulated cells and quantified with Bicinchoninic Acid (BCA) Protein Assay Kit (P0012s, Beyotime, China). After extraction, proteins were separated by sodium dodecyl sulfate-polyacrylamide gel electrophoresis

(SDS-PAGE; GenScript, USA) and transferred to polyvinylidene difluoride membranes (PVDF; Bio-Rad, USA). The membranes were blocked using 5% nonfat milk and incubated at 4°C with primary antibodies: rabbit anti-p16 (CST, 1:1000), rabbit anti-p53 (CST, 1:1000), rabbit anti-p65 (BOSTER, 1:800), rabbit anti-p-p65 (CST, 1:1000), mouse anti-p21 (SANTA, 1:400), and mouse anti-GAPDH (SANTA, 1:400). The membranes were then incubated with secondary antibodies (goat anti-rabbit, BOSTER, 1:2000; goat anti-mouse, BOSTER, 1:1500) for 1 h at 37°C. Protein bands were visualized using an Odyssey CLX Imaging system (LI-COR, USA) and analyzed with *ImageJ* software (version 1.8.0).

2.3 | Statistical Analysis

Each experiment was independently repeated at least three times. Quantitative data are expressed as mean \pm standard deviation and analyzed in *SPSS* software (version 26.0). *GraphPad Prism* software (version 9.4.0) was used for statistical analysis and visual representations. When the experimental design involves a single independent variable, overall differences are first assessed with a one-way ANOVA; when two independent variables are present, a two-way ANOVA is conducted. If the ANOVA indicates significance, post hoc comparisons are carried out while controlling the family-wise error rate (FWER). Tukey's post hoc test, which relies on the studentized-range (q) distribution, is used for all pairwise contrasts, whereas Dunnett's post hoc test, based on the multivariate t distribution, is applied for "many-to-one" comparisons in which each treatment group is evaluated against a common control. All multiplicity-adjusted p -values were calculated automatically in *GraphPad Prism* 9.4. Statistical significance was set at $p < 0.05$.

3 | Results

3.1 | Network Pharmacology Analysis

3.1.1 | Active Components and Targets of PR

A total of 56 chemical constituents of *PR* were collected through database searches. These constituents were screened using the criteria of OB $\geq 30\%$ and DL ≥ 0.18 , with additional information from literature sources. Ultimately, 20 putative active constituents of *PR* were predicted (Table 1), collectively predicted to target 329 different proteins. Notably, pseudoginsenoside F11 was excluded from the analysis due to the absence of predicted targets across four databases.

3.1.2 | Acquisition of Potential Therapeutic Targets

Through an extensive database search, we identified 2459 periodontitis-related targets and 2561 aging-related targets. By intersecting these with the targets of *PR*'s active constituents, we aimed to identify potential therapeutic targets for *PR* in counteracting the senescence of PDLSCs. This analysis revealed 90 candidate therapeutic targets that may mediate *PR*'s effects on PDLSC senescence (Figure 2A).

TABLE 1 | Bioactive compounds from *Polygonati Rhizoma (PR)*: Physicochemical data, oral bioavailability (OB), and drug-likeness (DL).

PubChem CID	Compound name	Molecular weight (g/mol)	Molecular formula	OB (%)	DL
222284	Beta-Sitosterol	414.7	C ₂₉ H ₅₀ O	36.91	0.75
10380176	(R)-Isomucronulatol	302.32	C ₁₇ H ₁₈ O ₅	67.67	0.26
114829	Liquiritigenin	256.25	C ₁₅ H ₁₂ O ₄	32.76	0.18
5281605	Baicalein	270.24	C ₁₅ H ₁₀ O ₅	33.52	0.21
5319422	3'-Methoxydaidzein	284.26	C ₁₆ H ₁₂ O ₅	48.57	0.24
162818391	(1R,2S,4R,6R,7S,8S,9R,12R,13R,16S)-6-[(3S)-4-hydroxy-3-methylbutyl]-6-methoxy-7,9,13-trimethyl-5-oxapentacyclo[10.8.0.0.02,9.04,8.013,18]icos-18-en-16-ol	446.7	C ₂₈ H ₄₆ O ₄	35.12	0.86
928837	(2R)-7-hydroxy-2-(4-hydroxyphenyl)-2,3-dihydrochromen-4-one	256.25	C ₁₅ H ₁₂ O ₄	71.12	0.18
165521	4',5-Dihydroxyflavone	254.24	C ₁₅ H ₁₀ O ₄	48.55	0.19
443024	Acanthoside B	580.6	C ₂₈ H ₃₆ O ₁₃	43.35	0.77
21633072	Pseudoginsenoside FII	801	C ₄₂ H ₇₂ O ₁₄	22.77	0.19
441207	Digitoxin	764.9	C ₄₁ H ₆₄ O ₁₃	—	—
15599558	Soyacerebroside II	714	C ₄₀ H ₇₅ N ₉ O	—	—
11775688	3-(butoxymethyl)-6,7-dihydro-5H-indolizin-8-one	221.29	C ₁₃ H ₁₉ N ₂ O	—	—
11499272	Kiancdmzgmial-uhfffaoya—	165.19	C ₉ H ₁₁ N ₂ O	—	—
3013842	3-Ethoxymethyl-5,6,7,8-tetrahydroindolizin-8-one	193.24	C ₁₁ H ₁₅ N ₂ O	—	—
5280863	Kaempferol	286.24	C ₁₅ H ₁₀ O ₆	41.88	0.24
5281672	Myricetin	318.23	C ₁₅ H ₁₀ O ₈	13.75	0.31
92095	Sarsasapogenin	416.6	C ₂₇ H ₄₄ O ₃	17.41	0.81
9898279	Ginsenoside Rb1	1109.3	C ₅₄ H ₉₂ O ₂₃	6.24	0.04
99474	Diosgenin	414.6	C ₂₇ H ₄₂ O ₃	80.88	0.81

3.1.3 | Construction of PPI Network and Identification of Core Targets

The therapeutic targets were imported into the STRING database to construct a PPI network. Network topology parameters, including DC, CC, and BC, were calculated using the *cytoHubba* plugin in *CytoScape*. The resulting PPI network contained 86 nodes and 700 edges, with node size determined by decreasing DC, as shown in Figure 2B. Cluster analysis using the *MCODE* plugin identified four network clusters comprising 42 nodes. The average DC, CC, and BC of these clusters were 16.28, 46.78, and 94.09, respectively, significantly higher than the overall network averages. As a result, these 42 nodes were designated as key predicted targets for *PR*'s role in counteracting the senescence of PDLSCs. The highest-scoring network cluster consisted of 21 nodes, with average DC, CC, and BC values of 34.38, 58.63, and 217.59, respectively (Figure 2C–F, Table 2). For subsequent

analyses, putative core targets were defined as those within the highest-scoring core cluster.

3.1.4 | GO Enrichment Analysis of Key Targets of the PPI Network

The 42 key targets of the PPI network were analyzed using the *clusterProfiler* package in *R* 4.3.2, yielding 2054 entries: 1954 in biological processes (BP), 84 in cellular components (CC), and 16 in molecular functions (MF). Figure 3B highlights the top ten significantly enriched entries across these categories. The BP category is enriched in pathways such as miRNA and ncRNA metabolism and the regulation of transcriptional processes. The MF category is associated with activities of ubiquitin-protein ligases and RNA- and DNA-binding transcription factors. The CC category is related to the structural activities of

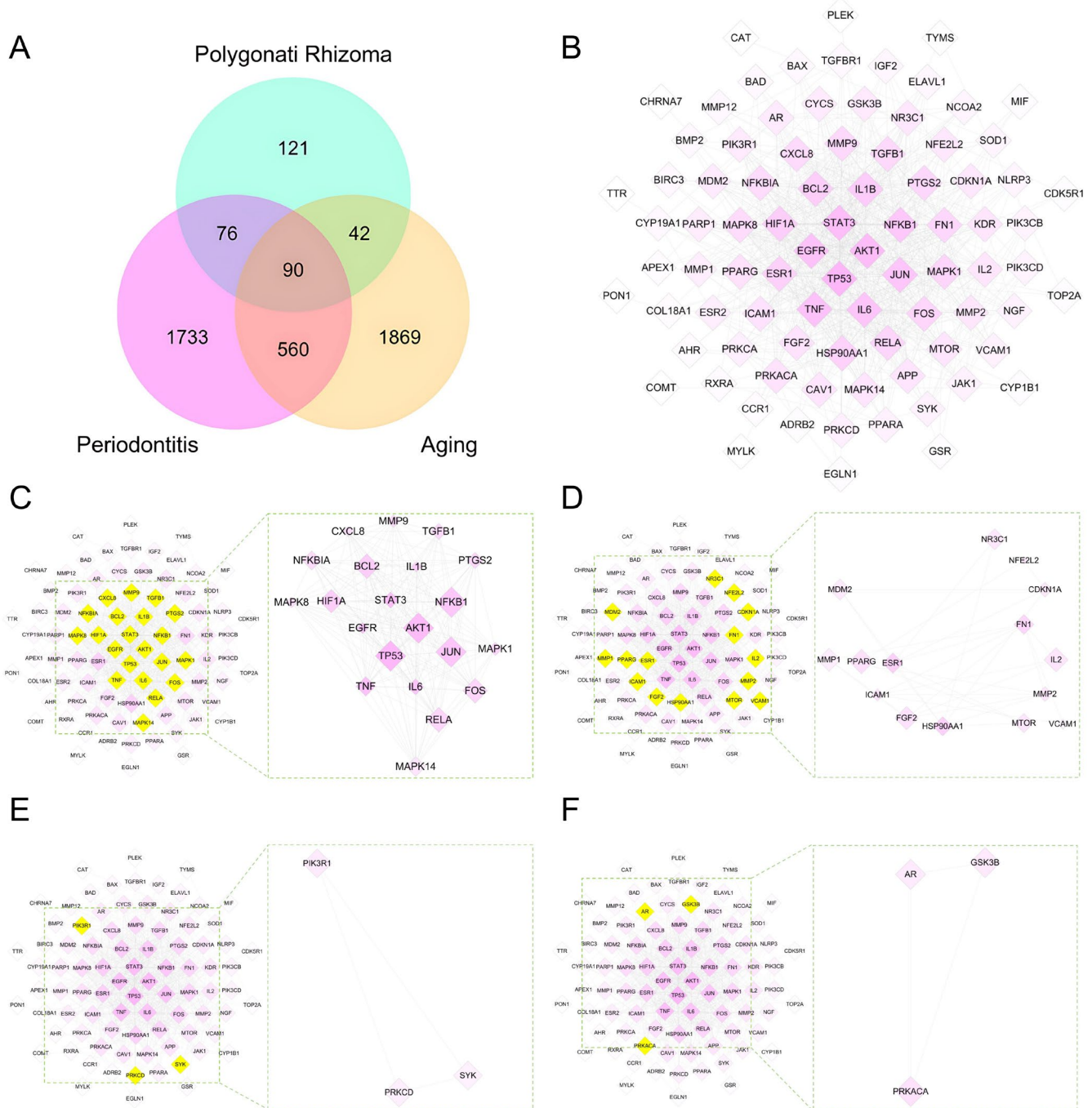


FIGURE 2 | Venn and PPI analyses of *Polygonati Rhizoma* (PR) anti-aging effects in periodontal ligament stem cells (PDLSCs). (A) Venn diagram of PR-modulated anti-aging targets in PDLSCs. (B) PPI network; node color intensity \propto degree centrality. (C) Top-scoring cluster: Left, full PPI with core targets in yellow; right, enlarged view. (D–F) Additional clusters from the clustering analysis.

the cellular vesicle lumen, secretory granule lumen, and other cellular structures.

3.1.5 | KEGG Enrichment Analysis of Key Targets of the PPI Network

We conducted KEGG pathway enrichment analysis of the key targets in the PPI network using the *clusterProfiler* package in R 4.3.2, identifying 146 pathways with a p value < 0.05 . This

analysis revealed 50 fundamental pathways and 96 disease-related pathways (Table 3). As shown in Figure 3A, the significantly enriched pathways are primarily involved in signal transduction, cell growth and death, development and regeneration, as well as pathways related to the immune, endocrine, and nervous systems. Cell growth and death-related pathways include those involved in cellular senescence and apoptosis. Signal transduction-related pathways encompass the NF- κ B signaling pathway (see Figure 3C) and the TNF signaling pathway.

TABLE 2 | Centrality metrics and MCODE scores for core targets in the PR-PDLSC PPI clusters.

	Target	MCODE Score	Degree	Closeness	Betweenness
Cluster 1					
	AKT1	14.63	47.00	65.00	659.26
	NFKB1	14.63	39.00	61.25	198.36
	TP53	14.63	50.00	66.75	813.01
	JUN	14.63	40.00	61.92	228.39
	FOS	13.89	30.00	56.42	66.51
	BCL2	13.89	35.00	59.08	214.29
	RELA	13.89	30.00	56.08	130.50
	HIF1A	13.74	35.00	58.75	182.51
	MAPK14	13.27	19.00	50.25	27.76
	TNF	13.23	43.00	63.08	428.41
	NFKBIA	13.18	25.00	53.58	68.98
	PTGS2	12.82	28.00	55.08	46.30
	TGFB1	12.81	27.00	54.92	129.41
	STAT3	12.81	46.00	64.75	341.61
	IL6	12.81	41.00	61.75	253.43
	MAPK1	12.46	30.00	56.92	127.59
	MMP9	12.38	27.00	54.75	82.82
	EGFR	12.20	43.00	63.25	299.38
	MAPK8	12.15	25.00	54.25	61.75
	IL1B	12.09	36.00	59.75	166.35
	CXCL8	12.06	26.00	53.75	42.85
Average		13.25	34.38	58.63	217.59
Cluster 2					
	PPARG	11.12	22.00	52.25	106.42
	IL2	11.10	18.00	49.12	12.05
	FGF2	11.03	21.00	51.08	30.99
	MMP1	11.00	13.00	45.28	0.86
	NR3C1	10.86	17.00	49.58	56.16
	MDM2	10.86	15.00	47.92	2.77
	ESR1	10.81	33.00	58.00	313.84
	FN1	10.76	28.00	55.08	218.22
	HSP90AA1	10.72	32.00	57.83	421.88
	MTOR	10.72	19.00	50.08	42.06
	MMP2	10.37	18.00	49.08	38.58
	CDKN1A	10.37	17.00	49.08	6.82
	ICAM1	10.17	21.00	51.08	14.40
	VCAM1	10.00	11.00	43.78	0.26

(Continues)

TABLE 2 | (Continued)

	Target	MCODE Score	Degree	Closeness	Betweenness
	NFE2L2	9.85	17.00	49.42	114.42
Average		10.65	20.13	50.58	91.98
Cluster 3	AR	8.84	15.00	48.33	53.25
	PRKACA	8.00	20.00	49.75	234.21
	GSK3B	7.42	16.00	49.25	43.81
Average		8.08	17.00	49.11	110.42
Cluster 4	PIK3R1	5.41	15.00	48.08	41.79
	PRKCD	5.00	12.00	45.75	31.96
	SYK	5.00	11.00	44.12	22.79
Average		5.14	12.67	45.98	32.18

3.1.6 | Molecular Docking

Through comprehensive analysis, including network clustering, GO and KEGG enrichment studies, and a review of existing literature, we identified tumor protein p53 (*TP53*), transcription factor p65 (*RELA*), tumor necrosis factor- α (*TNF- α*), transforming growth factor- β 1 (*TGF- β 1*), interleukin-6 (*IL-6*), matrix metalloproteinase-9 (*MMP-9*), interleukin-1 β (*IL-1 β*), and C-X-C motif chemokine ligand 8 (*CXCL-8*) as putative core targets. These targets were used as the basis for molecular docking with the active constituents of *PR*. The docking results, presented in Table 4, indicate an average binding energy of -7.2 kcal/mol for the active components of *PR* against these core targets. The interaction between myricetin and IL-1 β exhibited the highest binding energy at -5.5 kcal/mol, whereas baicalein and *MMP-9* demonstrated the lowest binding energy at -9.7 kcal/mol. This suggests that the components of *PR* may have a high affinity for these key predicted targets, potentially leading to a more stable molecular conformation. Additionally, we thoroughly analyzed the interaction between baicalein and its primary target, confirming that baicalein effectively binds to its target mainly through van der Waals forces and hydrogen bonds, as illustrated in Figure 4.

3.1.7 | Core Biological Network of *PR* Counteracting Senescence in PDLSCs

By mapping the active compounds of *PR* to their core targets and key signaling pathways, we constructed a putative core biological network through which *PR* may counteract the senescence of PDLSCs. As illustrated in Figure 5, *PR* exerts its anti-aging effects on PDLSCs through a synergistic action on multiple components, targets, and pathways.

3.2 | Verification Experiments

3.2.1 | Identification and Purification of PDLSCs

Periodontal ligament tissues were scraped from the apical third of the root surface. The cells were isolated using the tissue block method and observed under an inverted phase-contrast

microscope after approximately one week. A small number of cells were seen migrating from the edges of the tissue blocks, exhibiting a spindle shape with plump bodies and centrally located round or oval nuclei (Figure 6A). After about two weeks, the cells proliferated and migrated radially, forming radiating cell colonies around the tissue block (Figure 6B). Multiple monoclonal cell lines were combined using limited dilution, and the cultures were expanded. Within 24 h post-passage, the cells adhered, displayed normal morphology, exhibited good growth, and formed a spiral arrangement (Figure 6C). Third-generation cells were used for subsequent experiments. The methods and results of cell identification followed the procedures published by our previous research (Jing et al. 2024).

3.2.2 | Effect of D-Gal on PDLSC Activity

The CCK-8 assay was used to assess the effects of 5, 10, 20, and 40 g/L D-Gal on the viability of PDLSCs at 0, 24, and 48 h. The results indicated that D-Gal inhibited PDLSC viability in a time- and concentration-dependent manner. After 0 h, there was no significant difference in PDLSC viability across the groups. However, after 24 h of treatment, PDLSC viability in the 40 g/L D-Gal group was significantly reduced compared to the control group ($p < 0.05$). After 48 h of treatment, PDLSC viability in the 10, 20, and 40 g/L D-Gal groups was significantly lower than in the control group ($p < 0.05$, $p < 0.0001$, and $p < 0.0001$, respectively) (Figure 6D).

3.2.3 | Effect of D-Gal on PDLSC Senescence

SA- β -Gal staining was used to assess the effects of 5, 10, 20, and 40 g/L D-Gal on PDLSC senescence after 48 h of treatment. The results showed no significant difference in the SA- β -Gal positivity rate between the 5 g/L D-Gal group and the control group after 48 h. However, the SA- β -Gal positivity rates in the 10, 20, and 40 g/L D-Gal groups were significantly increased ($p < 0.001$, $p < 0.0001$, and $p < 0.0001$, respectively) in a concentration-dependent manner. Notably, in the 40 g/L D-Gal group, where cell growth was inhibited, the total number of cells was significantly reduced, yet the SA- β -Gal positivity rate continued to increase (Figure 6E,F).

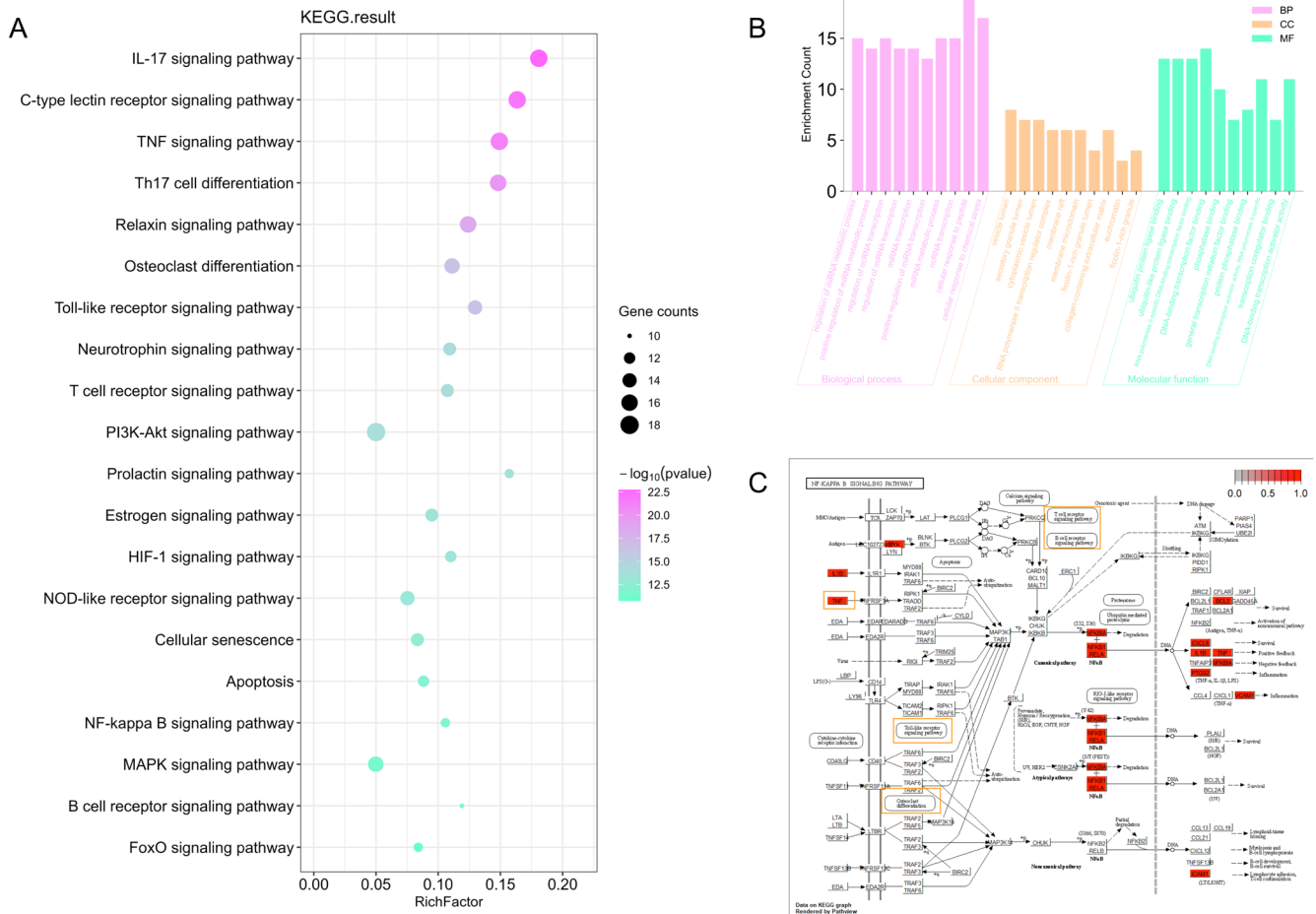


FIGURE 3 | GO/KEGG enrichment and pathway mapping. (A) KEGG enrichment of key targets (top 20). (B) GO enrichment of key targets. (C) Mapping of enriched targets in the NF-κB signaling pathway.

3.2.4 | Determining the Blood-Entry Components of PR-Medicated Serum

HPLC was used to analyze the components of PR-medicated serum. The results revealed that the average retention times for the standards myricetin, kaempferol, baicalein, β-sitosterol, and diosgenin were 15.215, 25.118, 23.815, 34.041, and 39.592 min, respectively. The corresponding peak wavelengths were 270, 360, 254, 210, and 203 nm. By comparing these retention times with the reference standards, it was confirmed that myricetin, kaempferol, baicalein, β-sitosterol, and diosgenin were present in the PR-medicated serum. The overall chromatographic profile, including peak numbers and resolution, indicated that the experimental conditions were optimal, with high stability and reproducibility (Figure 6G).

3.2.5 | Impact of PR-Medicated Serum on PDLSC Activity

The CCK-8 assay was used to assess the effects of 5%, 10%, 15%, and 20% PR-medicated serum on PDLSC viability at 0, 24, and 48 h. At 0 h, there was no significant difference in PDLSC viability among the groups. After 24 and 48 h of treatment, the 5% PR-medicated serum group exhibited the highest PDLSC viability, although the difference was not statistically significant.

After 48 h of treatment, the viability of PDLSCs in the 15% and 20% PR-medicated serum groups was significantly reduced compared to the control group ($p < 0.05$ and $p < 0.01$, respectively) (Figure 6H).

3.2.6 | Impact of Blank Serum on PDLSC Activity

The CCK-8 assay was used to assess the effects of 5%, 10%, 15%, and 20% blank serum on PDLSC viability at 0, 24, and 48 h. The results indicated that after 0 and 24 h of blank serum treatment, there were no significant differences in PDLSC viability among the groups. However, after 48 h of treatment, the viability of PDLSCs in the 15% and 20% blank serum groups was significantly lower compared to the control group ($p < 0.01$ and $p < 0.001$, respectively) (Figure 6I).

3.2.7 | Intracellular Oxidative Stress of PDLSCs

ROS staining was used to assess oxidative stress in PDLSCs following the experimental grouping. The results indicated that ROS levels in the D-Gal group were significantly higher than in the control group ($p < 0.001$). However, ROS levels in both the PR-medicated serum + D-Gal group and the Met + D-Gal group were significantly lower than those in the D-Gal group

TABLE 3 | Significantly enriched KEGG pathways for key targets in the PR-PDLSC PPI network.

Category	Subcategory	ID	Description	Count	p-value
Organismal systems	Immune system	hsa04657	IL-17 signaling pathway	17	1.80E-23
Organismal systems	Immune system	hsa04625	C-type lectin receptor signaling pathway	17	1.14E-22
Environmental information processing	Signal transduction	hsa04668	TNF signaling pathway	17	6.02E-22
Organismal systems	Immune system	hsa04659	Th17 cell differentiation	16	1.38E-20
Organismal systems	Endocrine system	hsa04926	Relaxin signaling pathway	16	2.72E-19
Organismal systems	Development and regeneration	hsa04380	Osteoclast differentiation	15	2.43E-17
Organismal systems	Immune system	hsa04620	Toll-like receptor signaling pathway	14	3.65E-17
Organismal systems	Nervous system	hsa04722	Neurotrophin signaling pathway	13	5.81E-15
Organismal systems	Immune system	hsa04660	T cell receptor signaling pathway	13	7.26E-15
Environmental information processing	Signal transduction	hsa04151	PI3K-Akt signaling pathway	18	1.22E-14
Organismal systems	Endocrine system	hsa04917	Prolactin signaling pathway	11	1.49E-14
Organismal systems	Endocrine system	hsa04915	Estrogen signaling pathway	13	3.76E-14
Environmental information processing	Signal transduction	hsa04066	HIF-1 signaling pathway	12	6.86E-14
Organismal systems	Immune system	hsa04621	NOD-like receptor signaling pathway	14	8.48E-14
Cellular processes	Cell growth and death	hsa04218	Cellular senescence	13	2.06E-13
Cellular processes	Cell growth and death	hsa04210	Apoptosis	12	1.02E-12
Environmental information processing	Signal transduction	hsa04064	NF-kappa B signaling pathway	11	1.37E-12

TABLE 4 | Docking affinities of PR compounds with key protein targets.

PubChem CID	Compound name	Target	PDB ID	Affinity (kcal/mol)
5280863	Kaempferol	CXCL8	5D14	-7.1
5281672	Myricetin	IL1B	6Y8M	-5.5
5281672	Myricetin	IL6	1ALU	-6
5280863	Kaempferol	MMP9	5IL2	-9.6
5281605	Baicalein	MMP9	5IL2	-9.7
99474	Diosgenin	RELA	3GUT	-7.3
5281605	Baicalein	RELA	3GUT	-5.8
222284	Beta-Sitosterol	TGFB1	5VQP	-6.6
5280863	Kaempferol	TNF	2AZ5	-7.3
5281672	Myricetin	TNF	2AZ5	-7.3
99474	Diosgenin	TP53	6GGC	-6.6
5281605	Baicalein	TP53	6GGC	-7.7

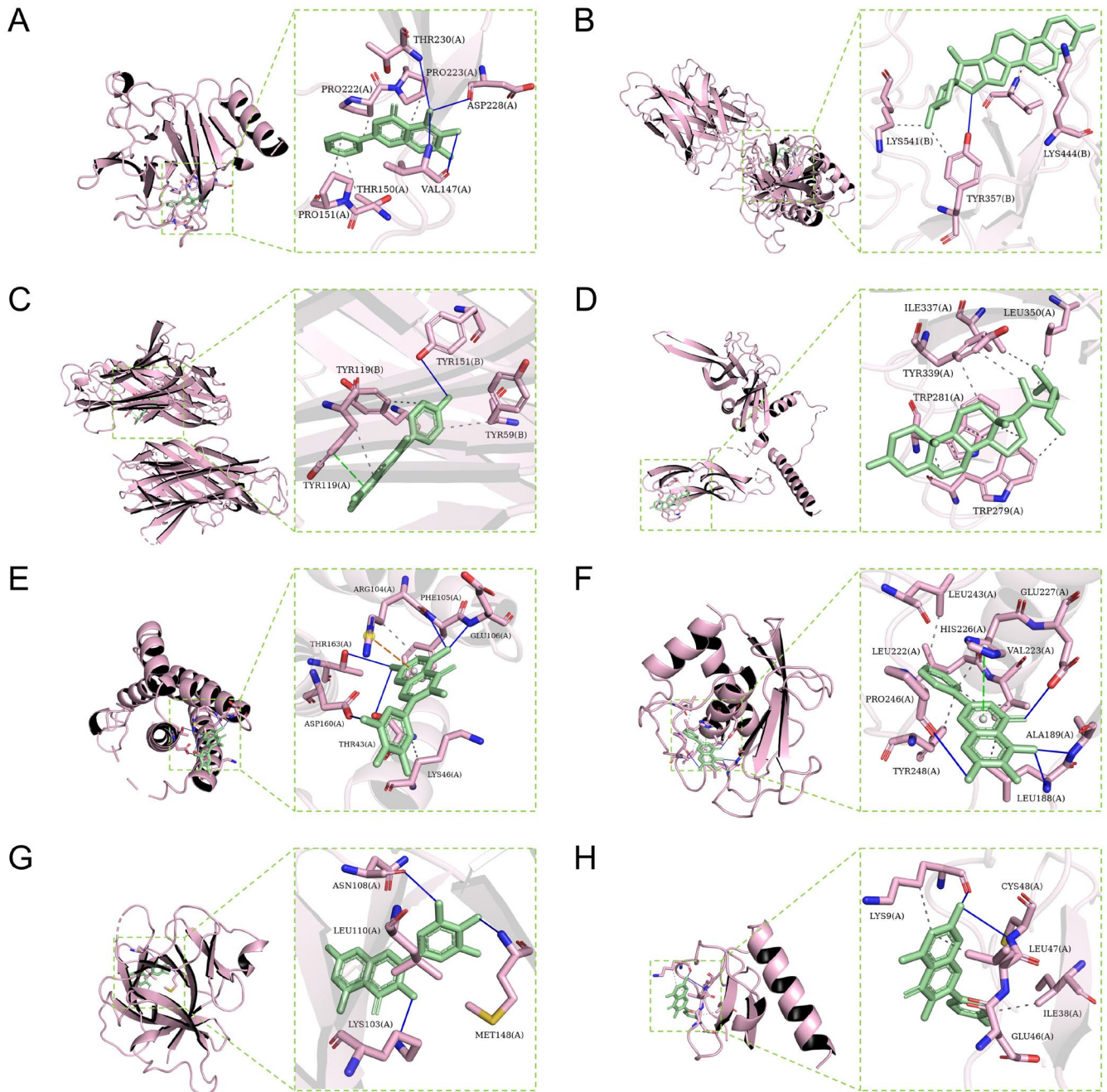


FIGURE 4 | Molecular docking between active PR components and core targets. (A) Baicalein-TP53; (B) Diosgenin-RELA; (C) Kaempferol-TNF- α ; (D) β -Sitosterol-TGF- β 1; (E) Myricetin-IL-6; (F) Baicalein-MMP-9; (G) Myricetin-IL-1 β ; (H) Kaempferol-CXCL-8.

(both $p < 0.01$). There was no significant difference in ROS levels between the PR-mediated serum + D-Gal group and the Met + D-Gal group (Figure 7A,D).

3.2.8 | Senescence of PDLSCs

SA- β -Gal staining was utilized to assess PDLSC senescence following the experimental grouping. The results showed that the SA- β -Gal positivity rate in the D-Gal group was significantly higher than that in the control group ($p < 0.001$). However, the SA- β -Gal positivity rates in both the PR-mediated serum + D-Gal group and the Met + D-Gal group were significantly lower than those in the D-Gal group (both $p < 0.05$). There was no

significant difference in the SA- β -Gal staining positivity rate between the PR-mediated serum + D-Gal group and the Met + D-Gal group (Figure 7B,E).

3.2.9 | Cell Cycle of PDLSCs

Flow cytometry was used to analyze the cell cycle distribution in PDLSCs following the experimental grouping. The results showed that the proportion of cells in the G₀/G₁ phase was significantly higher in the D-Gal group than in the control group ($p < 0.01$). Conversely, the proportion of G₀/G₁ phase cells in both the PR-mediated serum + D-Gal group and the Met + D-Gal group was significantly lower than that in the D-Gal group

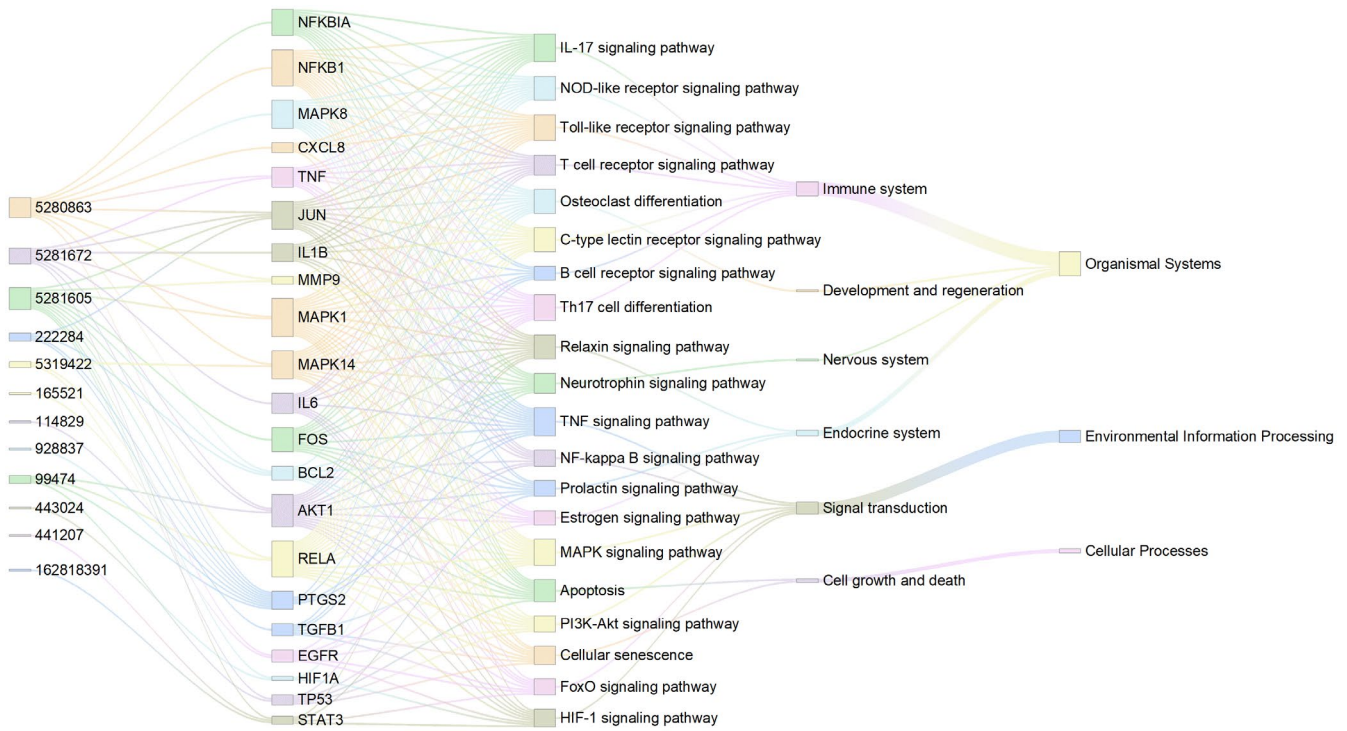


FIGURE 5 | Integrated mechanism by which *PR* counteracts PDLSC senescence.

(both $p < 0.001$). No significant difference in the proportion of G_0/G_1 phase cells between the *PR*-medicated serum + D-Gal group and the Met + D-Gal group (Figure 7C,F).

3.2.10 | The Protein Secretion Levels of SASP

ELISA was used to measure the protein secretion levels of pro-inflammatory factors (TNF- α , IL-6, and IL-1 β), growth factor TGF- β 1, the matrix metalloproteinase MMP-9, and the chemokine CXCL-8 within the SASP, following the experimental grouping. The D-Gal group exhibited significantly higher protein secretion levels of TNF- α , IL-6, IL-1 β , TGF- β 1, MMP-9, and CXCL-8 than the control group ($p < 0.001$, $p < 0.01$, $p < 0.001$, $p < 0.01$, $p < 0.001$, and $p < 0.001$, respectively). In the *PR*-medicated serum + D-Gal group, the secretion levels of these proteins were significantly lower than in the D-Gal group (all $p < 0.05$). Similarly, in the Met + D-Gal group, the protein secretion levels were significantly lower than in the D-Gal group ($p < 0.01$, $p < 0.05$, $p < 0.01$, $p < 0.001$, and $p < 0.01$, respectively). Furthermore, the Met + D-Gal group showed a significantly lower secretion of MMP proteins compared to the *PR*-medicated serum + D-Gal group ($p < 0.05$). No significant differences in protein secretion levels were observed between the Met + D-Gal group and the control group (Figure 8).

3.2.11 | The Protein Expression Levels of Molecular Markers Related to Cellular Senescence and the NF- κ B Signaling Pathway

Western blot analysis was used to detect the protein expression levels of cellular senescence markers p16, p21, and p53, as well as key signaling pathway components NF- κ B and p-NF- κ B,

following the experimental grouping. The results demonstrated that the protein expression levels of p16, p21, p53, and p-NF- κ B were significantly higher in the D-Gal group compared with the control group (all $p < 0.001$). In the *PR*-medicated serum + D-Gal group, the expression levels of these proteins were significantly lower than those in the D-Gal group ($p < 0.05$, $p < 0.01$, $p < 0.01$, and $p < 0.05$, respectively). Similarly, in the Met + D-Gal group, protein expression levels were significantly reduced compared with the D-Gal group ($p < 0.01$, $p < 0.01$, $p < 0.01$, and $p < 0.05$, respectively). No significant differences were observed in the expression levels of these proteins between the Met + D-Gal group and the *PR*-medicated serum + D-Gal group (Figure 9).

4 | Discussion

Over recent decades, significant efforts have been made in identifying and characterizing stem cells derived from dental tissues, including dental pulp stem cells (DPSCs), stem cells isolated from human pulp of exfoliated deciduous teeth (SHED), PDLSCs, stem cells from apical papilla (SCAPs), and dental follicle progenitor cells (DFPCs) (Zhai et al. 2019). PDLSCs were first identified in 2004 by Seo et al. (Seo et al. 2004) using stem cell markers STRO-1 (mesenchymal stromal-cell surface antigen) and cluster of differentiation 146 (CD146, also known as MCAM/MUC18). PDLSCs are notable for their self-renewal capacity, multipotency (including osteogenic, adipogenic, chondrogenic, and myogenic differentiation), and immunomodulatory properties (Bartold and Gronthos 2017; Hu et al. 2018; Nuñez et al. 2019).

In this study, PDLSCs were successfully isolated from the apical third of the root surface using the tissue block method and limiting dilution method. Our research group previously

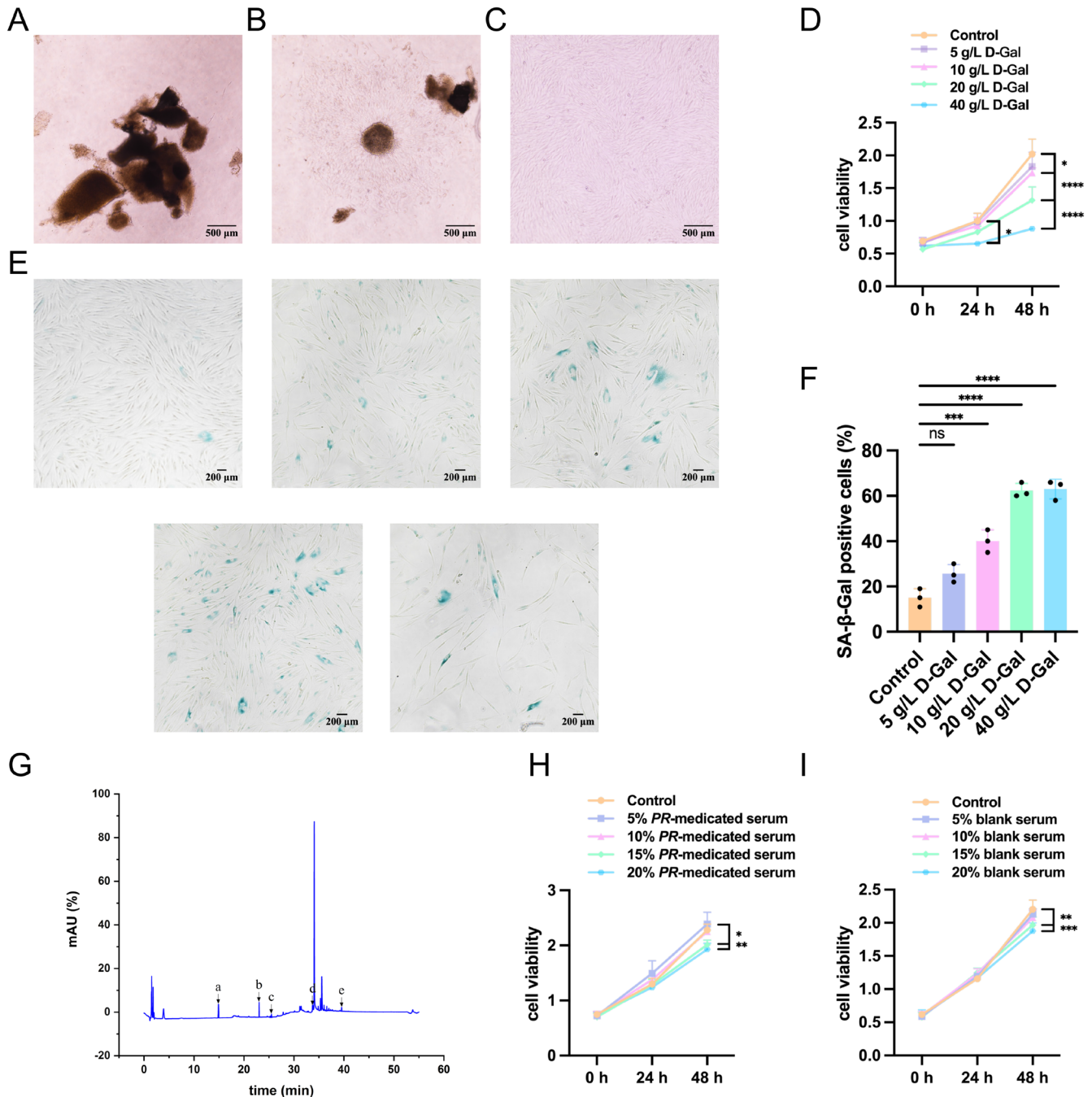


FIGURE 6 | Model establishment and serum characterization. (A) 1 week: Few cells migrate from periodontal ligament tissue block edge (40×). (B) 2 weeks: Radial colony forms around the block (40×). (C) Post-passage cells retain normal morphology with whirlpool-like arrangement (100×). (D) PDLSC viability after D-galactose exposure (CCK-8). (E) SA-β-Gal staining after 48 h with 5, 10, 20, 40 g/L D-galactose; Senescent cells in blue (100×). (F) Quantification of SA-β-Gal-positive cells. (G) HPLC chromatogram of PR-mediated serum: a, myricetin; b, kaempferol; c, baicalin; d, β-sitosterol; e, diosgenin. (H) Effect of PR-mediated serum on viability (CCK-8). (I) Effect of blank serum on viability (CCK-8). (Statistics: D, H, I two-way ANOVA with Dunnett's post hoc; F one-way ANOVA with Tukey's post hoc; * $p < 0.05$, ** $p < 0.01$, *** $p < 0.001$, **** $p < 0.0001$; ns, not significant).

demonstrated that these cells expressed positive markers for mesenchymal origin (STRO-1, CD146, CD29 [integrin β1], CD90 [Thy-1], and CD105 [endoglin]) and negative markers for hematopoietic origin (CD45 [protein tyrosine phosphatase receptor type C] and CD34 [hematopoietic progenitor cell antigen CD34]). Additionally, they exhibit the potential for osteogenic and adipogenic differentiation, meeting the identification criteria for PDLSCs (Pan et al. 2017).

D-Gal is a well-established senescence-inducing agent, commonly used to create aging models in vivo and in vitro. At normal concentrations, D-Gal is oxidized into glucose, but at elevated levels, it converts into aldohexose and hydrogen peroxide, generating large amounts of ROS. Additionally, D-Gal can be converted into galactitol, which disrupts cellular osmotic pressure, causing swelling and dysfunction, thereby inducing primary cell senescence (Zhang et al. 2009). D-Gal also reacts

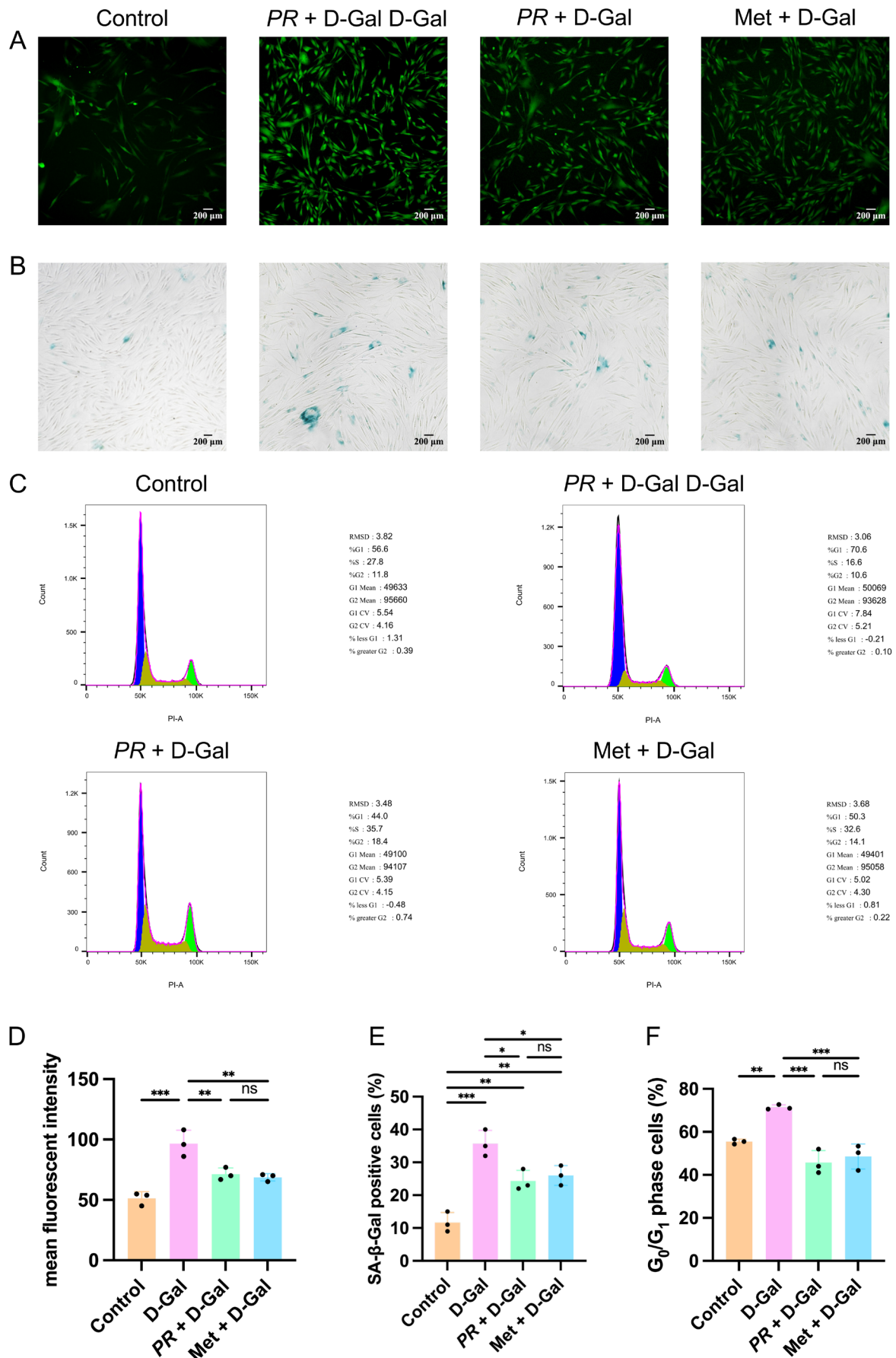


FIGURE 7 | Legend on next page.

FIGURE 7 | Senescence phenotyping. (A) ROS staining (green intensity reflects ROS; 100×). (B) SA-β-Gal staining (senescent cells in blue; 100×). (C) Cell-cycle distribution by flow cytometry. (D) Mean fluorescence intensity. (E) SA-β-Gal-positive rate. (F) G_0/G_1 fraction. (One-way ANOVA with Tukey's post hoc for D-F; significance as in Figure 6).

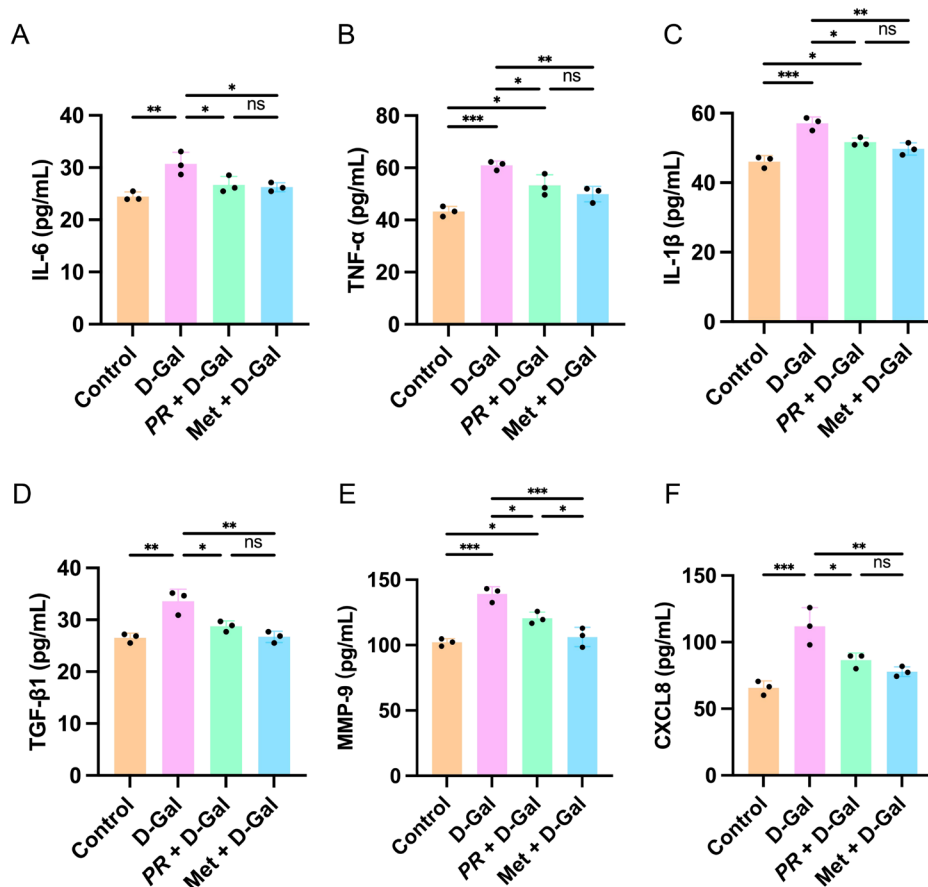


FIGURE 8 | ELISA of senescence-associated secretory phenotype factors. Secretion levels of (A) TNF-α, (B) IL-6, (C) IL-1β, (D) TGF-β1, (E) MMP-9, (F) CXCL-8. (One-way ANOVA with Tukey's post hoc; significance as in Figure 6).

with free amino groups in peptides and proteins to form advanced glycation end products (AGEs) (Cui et al. 2006). AGEs can stimulate cells to produce ROS through various pathways, particularly by promoting Nox2 expression via the NADPH oxidase pathway, resulting in a substantial increase in ROS (Zhang et al. 2006). This activates downstream NF-κB signaling pathways and the expression of SASP-associated cytokines, inducing secondary cell senescence (Schlett et al. 2023; Songkiatisak et al. 2022; Zhang et al. 2021). Using CCK-8 assays and SA-β-Gal staining, we established an in vitro PDLSC senescence model induced by 10 g/L D-Gal.

The research methodology for serum pharmacology in TCM involves orally administering the herbal medicine or its compounds to animals, followed by blood collection after a set period. The serum is then isolated and used to evaluate efficacy in vitro. This method avoids interference from the physical and chemical properties of crude herbal preparations and reflects the pharmacological effects of digestion, absorption, and biotransformation in the gastrointestinal tract (Bochu et al. 2005). The optimal concentration of medicated serum is determined using “same dosage administration, same blood collection time,

varying volume fractions”. Most studies use volume fractions of 5%, 10%, 15%, and 20%. Too low a concentration can slow cell growth, while too high a concentration may lead to rapid cell growth, differentiation, aging, or inhibition of cell proliferation. The optimal concentration often varies depending on the cell type.

In this study, *PR* extract or saline solution was administered to rats, with blood collected and diluted in complete serum medium. CCK-8 assay results indicated that 5% *PR*-medicated serum and blank serum were appropriate for PDLSCs, while 15% and 20% concentrations significantly inhibited PDLSC viability. HPLC analysis confirmed the presence of myricetin, kaempferol, baicalein, β-sitosterol, and diosgenin in the *PR*-medicated serum, validating network pharmacology predictions.

Additionally, Met, a first-line treatment for type 2 diabetes (Scarpello and Howlett 2008), is known for its role in regulating glucose metabolism (Miller et al. 2013; Xenos et al. 2022), reducing inflammation (Moiseeva et al. 2013), exerting antioxidant activity (Forouzandeh et al. 2014; Polidori and Mecocci 2022), and delaying aging (Boehm and Slack 2006). It can also modulate

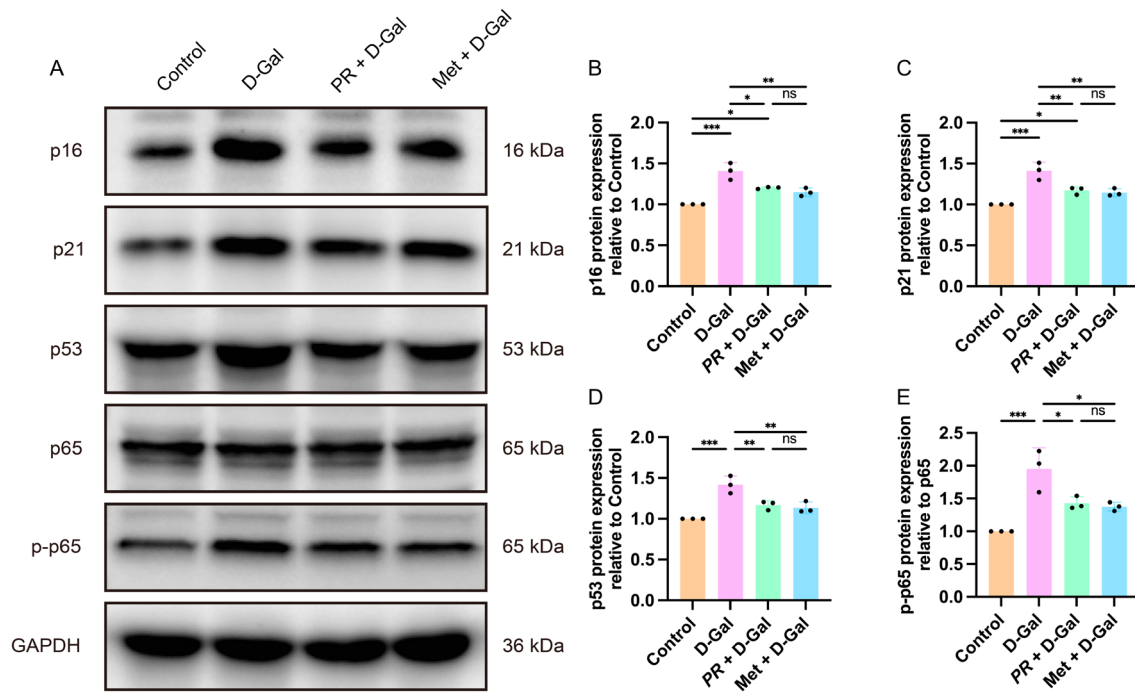


FIGURE 9 | Western blot of senescence markers and NF- κ B signaling. (A) Blot images. (B–E) Densitometry of p16, p21, p53, and phospho-p65. (One-way ANOVA with Tukey's post hoc; significance as in Figure 6).

the production of various SASP factors by inhibiting the NF- κ B signaling pathway (Wiley and Campisi 2021). Studies have shown that 100 μ M Met alleviates hydrogen peroxide-induced PDLSC senescence and restores osteogenic differentiation (Kuang et al. 2020). Based on these findings, 100 μ M Met was selected as the positive control for 5% PR-mediated serum in subsequent experiments.

Senescent MSCs display several hallmark changes, including a flattened, enlarged morphology, reduced proliferation and migration, increased ROS levels, elevated SA- β -Gal activity, and SASP secretion. They also experience cell cycle arrest, impaired multilineage differentiation, and reduced immunomodulatory and paracrine effects (Jiang et al. 2023).

In this study, we found that D-Gal treatment significantly increased ROS levels, SA- β -Gal activity, and the proportion of cells in the G₀/G₁ phase in PDLSCs. Treatment with PR-mediated serum or Met along with D-Gal significantly reduced ROS levels, SA- β -Gal activity, and the proportion of G₀/G₁ phase cells, with no significant difference observed between the two treatments. Assays verified that D-Gal triggered oxidative stress-mediated senescence in PDLSCs in vitro, while PR-mediated serum and Met effectively attenuated it.

As previously mentioned, the active constituents of PR have demonstrated potential in reducing inflammation and delaying aging (Zhao et al. 2023). However, the specific biomarkers and biological pathways through which these constituents address PDLSC senescence remain unclear. This study employed a systematic network pharmacology approach to elucidate the mechanisms by which PR combats the senescence of PDLSCs, and validated these findings experimentally. Our network pharmacology analysis identified 19 active PR components. Molecular

docking results indicated strong binding activities between the core targets and key active components, including baicalein, diosgenin, kaempferol, β -sitosterol, and yangmeinin.

Baicalein has been shown to promote the osteogenic differentiation of PDLSCs in both normal (Chen et al. 2017) and inflammatory (Ren et al. 2021) environments by activating the Wnt/ β -catenin signaling pathway. It also mitigates the inflammatory response induced by lipopolysaccharide (LPS) in PDLSCs by inhibiting the MAPK signaling pathway (Ren et al. 2021). Additionally, baicalein activates the Nrf2 signaling pathway, reducing high glucose-induced oxidative stress in human gingival epithelial cells (hGECs) and attenuating alveolar bone resorption in a diabetic periodontitis rat model (Zhu et al. 2020). Encapsulation of baicalein in nanoparticles (Li et al. 2017) and incorporation into chitosan/dioleoylphosphatidylethanolamine-baicalein nanohydrogels (Guo et al. 2024) has been effective in treating IL-1 β -induced hGECs and diabetic periodontitis rat models respectively, exhibiting significant anti-inflammatory effects.

Diosgenin was found to reduce the expression and secretion of inflammatory factors, such as IL-1 β , IL-6, and TNF- α , in LPS-induced PDLSCs and inhibit the nuclear translocation of NF- κ B p65 and phosphorylated I κ B- α (Cong et al. 2023). Studies using network pharmacology have also identified kaempferol and β -sitosterol as key active ingredients in periodontitis treatment, showing high binding affinity to B-cell lymphoma 2 (BCL2). In addition, surface-plasmon-resonance analyses have confirmed that kaempferol binds directly to human TNF- α and disrupts the TNF- α /TNFR1 interface, whereas cellular thermal-shift assays demonstrate that baicalein directly engages TP53 (Dou et al. 2024; Wang et al. 2022). Sinensis-angelica, which contains these compounds, has been shown to stimulate the expression of

osteogenesis-related genes and proteins in MC3T3-E1 cells, providing osteoprotective effects in periodontitis treatment (Chen et al. 2023). HPLC analysis of *PR*-medicated serum confirmed the presence of populin, kaempferol, baicalein, β -sitosterol, and diosgenin components, supporting the predictions made by network pharmacology analysis.

We identified a total of 8 key targets, including *TP53*, *RELA*, *TNF- α* , *TGF- β 1*, *IL-6*, *MMP-9*, *IL-1 β* , and *CXCL-8*, that *PR*'s active components may act on to mitigate PDLSC senescence. Molecular docking results revealed a high affinity between these hub genes and *PR*'s active constituents, suggesting their potential therapeutic relevance in combating PDLSC senescence. This study identified a total of 90 targets against PDLSC senescence, of which 42 were classified as key targets, and 21 were identified as core targets for the antagonistic effects of *PR* on PDLSC senescence.

PR antagonizes senescence in PDLSCs by targeting molecular markers of cellular senescence, including *TP53* and *RELA* (a key protein in the NF- κ B signaling pathway), as well as various cytokines associated with the SASP. These cytokines include pro-inflammatory factors such as *TNF- α* , *IL-6*, and *IL-1 β* , the growth factor *TGF- β 1*, the matrix metalloproteinase *MMP-9*, and the chemokine *CXCL-8*. *IL-6* is a prominent SASP factor (Cai et al. 2022), while *TNF- α* and *IL-1 β* are implicated in many inflammatory diseases and are key targets for anti-inflammatory therapies (Broderick and Hoffman 2022; Zelová and Hošek 2013). *TGF- β 1* regulates cell growth and differentiation (Richardson et al. 2023). *MMP-9* is vital for extracellular matrix metabolism (Rashid and Bardaweel 2023). *CXCL-8*, also known as *IL-8*, promotes tissue repair and infection resistance (Cambier et al. 2023).

Recent animal studies have shown that senescent PDLSCs can contribute to periodontitis development by exacerbating chronic inflammation and periodontal tissue destruction through the secretion of SASP factors (Ikegami et al. 2023). Therefore, targeting SASP factors secreted by senescent PDLSCs is an important strategy for adjunctive treatment of periodontitis. ELISA results showed a significant increase in the protein secretion of SASP factors following D-Gal treatment. In contrast, Met treatment led to a significant decrease in *MMP-9* protein secretion compared to *PR*-medicated serum, although no significant difference was observed between Met and the control group. Both *PR*-medicated serum and Met effectively down-regulated the secretion of SASP proteins, with Met demonstrating a stronger effect.

The regulation of SASP responses occurs at various levels, including transcription, mRNA stability, translation, and extracellular secretion. SASP activation is specifically mediated by innate immune signaling pathways, mechanistic target of rapamycin complex 1 (mTORC1), and transcription factors such as NF- κ B, CREB-binding protein (CBP), and GATA-binding protein 4 (GATA4) (Cai et al. 2022) (Songkiatisak et al. 2022).

KEGG pathway enrichment analysis identified several significantly enriched pathways, including cellular senescence and the NF- κ B signaling pathway. Although the NF- κ B signaling pathway may not be the most enriched pathway in network

pharmacology studies, it remains a critical regulator of a range of SASP factors. Additionally, p65, a key protein within the NF- κ B signaling pathway, is considered a core target.

NF- κ B plays a crucial role in regulating the activation of inflammatory T cells and proinflammatory factors within innate immunity. It also regulates T-cell differentiation and effector functions, making it essential for downstream inflammatory and immune-related signaling pathways (Lawrence 2009; Tak and Firestein 2001). Inhibition of NF- κ B signaling pathway activation has been shown to mitigate the inflammatory response in animal models of chronic periodontitis, reducing alveolar bone destruction (Wang et al. 2021). The NF- κ B signaling pathway is crucial in counteracting aging and limiting periodontitis-induced damage.

The NF- κ B family comprises c-Rel, RelA (p65), v-rel avian reticuloendotheliosis viral oncogene homolog B (RelB), NF- κ B1 (p50) and NF- κ B2 (p52). Notably, the phosphorylation of RelA (p65) is ROS-dependent and essential for transcriptional activation of target genes downstream of NF- κ B (Lingappan 2018).

Based on network pharmacology findings, it is hypothesized that PDLSC senescence is mediated through the NF- κ B pathway through promotion of SASP factor secretion. Western Blot analyses revealed a significant increase in protein expression levels of cellular senescence markers and NF- κ B pathway components following D-Gal treatment. However, these protein levels were significantly reduced by treatment with *PR*-medicated serum or Met, particularly when administered concurrently with D-Gal. Additionally, Met significantly reduced NF- κ B signaling protein expression compared to *PR*-medicated serum. Both *PR*-medicated serum and Met effectively downregulated markers associated with cellular senescence and the NF- κ B signaling pathway, with Met showing a more pronounced effect.

This study combines network pharmacology and experimental validation to explore the mechanisms by which *PR* mitigates oxidative stress-induced senescence in PDLSCs, offering a theoretical foundation for its use in periodontal tissue engineering and periodontitis treatment. However, inherent limitations exist due to the aggregation of heterogeneous datasets in network pharmacology, which may introduce information bias. Incompletely curated compound libraries may miss minor *PR* constituents, leading to false-negative target predictions, while target repositories biased toward oncology and immunology may overrepresent well-studied hubs such as *TP53* or *TNF- α* . Consequently, some of the 21 'core' targets may be over-ranked, and under-represented proteins may remain relevant. Additionally, static protein-interaction graphs cannot capture dynamic, tissue-specific, or feedback loop interactions, and thus, pathway readouts should be considered putative.

To address these issues, we (i) queried five independent databases, (ii) annotated targets using four in silico algorithms, (iii) confirmed compound-target interactions via molecular docking, and (iv) validated downstream signaling inhibition in senescent PDLSCs through Western blot and ELISA. Despite these efforts, all hypotheses remain provisional and require further validation. Molecular docking, which treats proteins as rigid, can misestimate binding affinities, and direct ligand-target interaction

evidence is limited (Desta et al. 2020; Huang and Zou 2010). Future studies should employ co-immunoprecipitation to confirm interactions between *PR* components and targets.

Although this study is based on in vitro assays, rodent models have confirmed *PR*'s efficacy against senescence and periodontitis (Huang et al. 2025; Pan et al. 2024; Wu et al. 2024; Zheng 2020). Our next phase will use a ligature-induced periodontitis mouse model to validate the NF- κ B mechanism and assess pharmacokinetics, dose optimization, and long-term safety.

Clinically, *PR* could be applied as a host-modulating gel or nanoparticle spray after scaling-and-root-planing (SRP) to promote inflammation resolution and bone regeneration. It may also be combined with low-dose chlorhexidine or doxycycline to enhance antibacterial and host-response effects while mitigating antibiotic resistance. Additionally, it could serve as a mouth rinse or muco-adhesive patch for early or maintenance therapy. A stepwise translational roadmap is proposed, starting with pre-clinical studies, followed by a dose-finding study in a periodontitis model, and concluding with a randomized controlled trial comparing SRP with and without *PR* gel.

5 | Conclusions

PR mitigates oxidative-stress-induced senescence in PDLSCs through multi-component, multi-target modulation predicted by our network-pharmacology workflow and experimentally validated. *PR*-medicated serum reduced oxidative damage, curtailed the SASP via the NF- κ B pathway, and performed comparably to metformin in most readouts, although metformin showed a slightly stronger suppression of SASP proteins. These findings position *PR* as a promising adjunct therapy for delaying PDLSC senescence and advancing periodontal tissue-engineering strategies, while the network pharmacology predictions also illuminate new putative avenues for anti-aging interventions in periodontitis.

Author Contributions

Xinran Feng: conceptualization, methodology, formal analysis, investigation, data curation, writing – original draft. **Ying An:** investigation, data curation, validation. **Fanfan Hou:** resources, methodology, technical support, data curation. **Qian Guo:** supervision, formal analysis, writing – review and editing. **Shanshan Cai:** supervision, validation, writing – review and editing. **Hongbin Xu:** supervision, conceptualization, writing – review and editing. **Youfu He:** supervision, project administration, writing – review and editing.

Acknowledgments

We are grateful to the public databases involved in this work.

Funding

The authors have nothing to report.

Ethics Statement

The experiment involving human tissues was approved by the Ethics Committee of School of Stomatology, China Medical University

(K2023007). The animal experiments were approved by the Ethics Commission of China Medical University, Shenyang, China (Approval No. CMU20231000).

Consent

The authors have approved the manuscript for submission.

Conflicts of Interest

The authors declare no conflicts of interest.

Data Availability Statement

The data that support the findings of this study are available from the corresponding author upon reasonable request.

References

- AgingAtlasConsortium. 2021. "Aging Atlas: A Multi-Omics Database for Aging Biology." *Nucleic Acids Research* 49, no. D1: D825–d830. <https://doi.org/10.1093/nar/gkaa894>.
- Aquino-Martinez, R. 2023. "The Emerging Role of Accelerated Cellular Senescence in Periodontitis." *Journal of Dental Research* 102, no. 8: 854–862. <https://doi.org/10.1177/00220345231154567>.
- Bader, G. D., and C. W. Hogue. 2003. "An Automated Method for Finding Molecular Complexes in Large Protein Interaction Networks." *BMC Bioinformatics* 4: 2. <https://doi.org/10.1186/1471-2105-4-2>.
- Baima, G., M. Romandini, F. Citterio, F. Romano, and M. Aimetti. 2022. "Periodontitis and Accelerated Biological Aging: A Geroscience Approach." *Journal of Dental Research* 101, no. 2: 125–132. <https://doi.org/10.1177/00220345211037977>.
- Bartold, P. M., and S. Gronthos. 2017. "Standardization of Criteria Defining Periodontal Ligament Stem Cells." *Journal of Dental Research* 96, no. 5: 487–490. <https://doi.org/10.1177/0022034517697653>.
- Behfarnia, P., S. Fazlalizadeh, M. H. Nasr-Esfahani, F. Ejeian, and A. Mogharehabet. 2023. "Isolation and Characterization of Human Periodontal Ligament Stem Cells Under the Terms of Use in Clinical Application: A Pilot Study." *Dent Res J (Isfahan)* 20: 105.
- Berman, H. M., J. Westbrook, Z. Feng, et al. 2000. "The Protein Data Bank." *Nucleic Acids Research* 28, no. 1: 235–242. <https://doi.org/10.1093/nar/28.1.235>.
- Bochu, W., Z. Liancai, and C. Qi. 2005. "Primary Study on the Application of Serum Pharmacology in Chinese Traditional Medicine." *Colloids and Surfaces. B, Biointerfaces* 43, no. 3–4: 194–197. <https://doi.org/10.1016/j.colsurfb.2005.04.013>.
- Boehm, M., and F. J. Slack. 2006. "MicroRNA Control of Lifespan and Metabolism." *Cell Cycle* 5, no. 8: 837–840. <https://doi.org/10.4161/cc.5.8.2688>.
- Broderick, L., and H. M. Hoffman. 2022. "IL-1 and Autoinflammatory Disease: Biology, Pathogenesis and Therapeutic Targeting." *Nature Reviews Rheumatology* 18, no. 8: 448–463. <https://doi.org/10.1038/s41584-022-00797-1>.
- Cai, Y., W. Song, J. Li, et al. 2022. "The Landscape of Aging." *Science China. Life Sciences* 65, no. 12: 2354–2454. <https://doi.org/10.1007/s11427-022-2161-3>.
- Cambier, S., M. Gouwy, and P. Proost. 2023. "The Chemokines CXCL8 and CXCL12: Molecular and Functional Properties, Role in Disease and Efforts Towards Pharmacological Intervention." *Cellular & Molecular Immunology* 20, no. 3: 217–251. <https://doi.org/10.1038/s41423-023-00974-6>.
- Chen, C. Y. 2011. "TCM Database@Taiwan: The World's Largest Traditional Chinese Medicine Database for Drug Screening in Silico."

- PLoS One 6, no. 1: e15939. <https://doi.org/10.1371/journal.pone.0015939>.
- Chen, L. J., B. B. Hu, X. L. Shi, et al. 2017. "Baicalein Enhances the Osteogenic Differentiation of Human Periodontal Ligament Cells by Activating the Wnt/ β -Catenin Signaling Pathway." *Archives of Oral Biology* 78: 100–108. <https://doi.org/10.1016/j.archoralbio.2017.01.019>.
- Chen, Q., Y. Wang, C. Shi, et al. 2023. "Molecular Mechanism of the Asarum-Angelica Drug Pair in the Treatment of Periodontitis Based on Network Pharmacology and Experimental Verification." *International Journal of Molecular Sciences* 24, no. 24: 17389. <https://doi.org/10.3390/ijms242417389>.
- Chen, X., H. Zhou, Y. B. Liu, et al. 2006. "Database of Traditional Chinese Medicine and Its Application to Studies of Mechanism and to Prescription Validation." *British Journal of Pharmacology* 149, no. 8: 1092–1103. <https://doi.org/10.1038/sj.bjp.0706945>.
- Cong, S., Q. Peng, L. Cao, et al. 2023. "Diosgenin Prevents Periodontitis by Inhibiting Inflammation and Promoting Osteogenic Differentiation." *Oral Diseases* 30: 2497. <https://doi.org/10.1111/odi.14708>.
- Cui, X., P. Zuo, Q. Zhang, et al. 2006. "Chronic Systemic D-Galactose Exposure Induces Memory Loss, Neurodegeneration, and Oxidative Damage in Mice: Protective Effects of R-Alpha-Lipoic Acid." *Journal of Neuroscience Research* 83, no. 8: 1584–1590. <https://doi.org/10.1002/jnr.20845>.
- Czesnikiewicz-Guzik, M., G. Osmenda, M. Siedlinski, et al. 2019. "Causal Association Between Periodontitis and Hypertension: Evidence From Mendelian Randomization and a Randomized Controlled Trial of Non-Surgical Periodontal Therapy." *European Heart Journal* 40, no. 42: 3459–3470. <https://doi.org/10.1093/eurheartj/ehz646>.
- Daina, A., O. Michielin, and V. Zoete. 2019. "SwissTargetPrediction: Updated Data and New Features for Efficient Prediction of Protein Targets of Small Molecules." *Nucleic Acids Research* 47, no. W1: W357–w364. <https://doi.org/10.1093/nar/gkz382>.
- Desta, I. T., K. A. Porter, B. Xia, D. Kozakov, and S. Vajda. 2020. "Performance and Its Limits in Rigid Body Protein-Protein Docking." *Structure* 28, no. 9: 1071–1081. <https://doi.org/10.1016/j.str.2020.06.006>.
- Dou, B., Y. Cui, Q. Zhou, et al. 2024. "Mechanism of Baicalein in Treatment of Castration-Resistant Prostate Cancer Based on Network Pharmacology and Cell Experiments." *Frontiers in Pharmacology* 15: 1397703. <https://doi.org/10.3389/fphar.2024.1397703>.
- Feng, X., D. Peng, Y. Qiu, et al. 2024. "Identification and Validation of Aging- and Endoplasmic Reticulum Stress-Related Genes in Periodontitis Using a Competing Endogenous RNA Network." *Inflammation* 48: 1326.
- Forouzandeh, F., G. Salazar, N. Patrushev, et al. 2014. "Metformin Beyond Diabetes: Pleiotropic Benefits of Metformin in Attenuation of Atherosclerosis." *Journal of the American Heart Association* 3, no. 6: e001202. <https://doi.org/10.1161/jaha.114.001202>.
- GeneOntologyConsortium. 2015. "Gene Ontology Consortium: Going Forward." *Nucleic Acids Research* 43: D1049–D1056. <https://doi.org/10.1093/nar/gku1179>.
2018. "Global, Regional, and National Incidence, Prevalence, and Years Lived With Disability for 354 Diseases and Injuries for 195 Countries and Territories, 1990–2017: A Systematic Analysis for the Global Burden of Disease Study 2017." *Lancet* 392, no. 10159: 1789–1858. [https://doi.org/10.1016/s0140-6736\(18\)32279-7](https://doi.org/10.1016/s0140-6736(18)32279-7).
- Guo, L., M. Han, H. Zhang, and Y. Han. 2024. "Effect of Chitosan/Dioleoyl Phosphatidyl Ethanolamine - Baicalein Nanohydrogel in the Treatment of Rat With Periodontitis." *Heliyon* 10, no. 3: e25209. <https://doi.org/10.1016/j.heliyon.2024.e25209>.
- Hu, L., Y. Liu, and S. Wang. 2018. "Stem Cell-Based Tooth and Periodontal Regeneration." *Oral Diseases* 24, no. 5: 696–705. <https://doi.org/10.1111/odi.12703>.
- Huang, R., R. Che, T. Sun, W. Xie, and S. Zhang. 2025. "Investigating the Renoprotective Effects of Polygonatum Sibiricum Polysaccharides (PSP) on D-Galactose-Induced Aging Mice: Insights From Gut Microbiota and Metabolomics Analyses." *Frontiers in Microbiology* 16: 1550971. <https://doi.org/10.3389/fmicb.2025.1550971>.
- Huang, S. Y., and X. Zou. 2010. "Advances and Challenges in Protein-Ligand Docking." *International Journal of Molecular Sciences* 11, no. 8: 3016–3034. <https://doi.org/10.3390/ijms11083016>.
- Ikegami, K., M. Yamashita, M. Suzuki, et al. 2023. "Cellular Senescence With SASP in Periodontal Ligament Cells Triggers Inflammation in Aging Periodontal Tissue." *Aging (Albany NY)* 15, no. 5: 1279–1305. <https://doi.org/10.18632/aging.204569>.
- Iwayama, T., H. Sakashita, M. Takedachi, and S. Murakami. 2022. "Periodontal Tissue Stem Cells and Mesenchymal Stem Cells in the Periodontal Ligament." *Japanese Dental Science Review* 58: 172–178. <https://doi.org/10.1016/j.jdsr.2022.04.001>.
- Jiang, X., W. Li, L. Ge, and M. Lu. 2023. "Mesenchymal Stem Cell Senescence During Aging: From Mechanisms to Rejuvenation Strategies." *Aging and Disease* 14, no. 5: 1651–1676. <https://doi.org/10.14336/ad.2023.0208>.
- Jing, Z., X. Feng, X. Li, X. Zhang, and C. Pan. 2024. "Vaspin Facilitates the Proliferation and Osteogenic Differentiation of Periodontal Ligament Stem Cells." *Journal of Periodontal Research* 59, no. 4: 812–820. <https://doi.org/10.1111/jre.13254>.
- Keiser, M. J., B. L. Roth, B. N. Armbruster, P. Ernsberger, J. J. Irwin, and B. K. Shoichet. 2007. "Relating Protein Pharmacology by Ligand Chemistry." *Nature Biotechnology* 25, no. 2: 197–206. <https://doi.org/10.1038/nbt1284>.
- Kinane, D. F., P. G. Stathopoulou, and P. N. Papapanou. 2017. "Periodontal Diseases." *Nature Reviews Disease Primers* 3: 17038. <https://doi.org/10.1038/nrdp.2017.38>.
- Kuang, Y., B. Hu, G. Feng, et al. 2020. "Metformin Prevents Against Oxidative Stress-Induced Senescence in Human Periodontal Ligament Cells." *Biogerontology* 21, no. 1: 13–27. <https://doi.org/10.1007/s10522-019-09838-x>.
- Lawrence, T. 2009. "The Nuclear Factor NF-kappaB Pathway in Inflammation." *Cold Spring Harbor Perspectives in Biology* 1, no. 6: a001651. <https://doi.org/10.1101/cshperspect.a001651>.
- Li, X., W. Luo, T. W. Ng, et al. 2017. "Nanoparticle-Encapsulated Baicalein Markedly Modulates Pro-Inflammatory Response in Gingival Epithelial Cells." *Nanoscale* 9, no. 35: 12897–12907. <https://doi.org/10.1039/c7nr02546g>.
- Liguori, I., G. Russo, F. Curcio, et al. 2018. "Oxidative Stress, Aging, and Diseases." *Clinical Interventions in Aging* 13: 757–772. <https://doi.org/10.2147/cia.S158513>.
- Lin, X.-J., Q. Yuan, J. Zhou, Y.-L. Dong, D. Sunchuri, and Z.-L. Guo. 2024. "Cellular Senescence: A New Perspective on the Suppression of Periodontitis (Review)." *Molecular Medicine Reports* 30, no. 6: 238. <https://doi.org/10.3892/mmr.2024.13362>.
- Lingappan, K. 2018. "NF- κ B in Oxidative Stress." *Current Opinion in Toxicology* 7: 81–86. <https://doi.org/10.1016/j.cotox.2017.11.002>.
- López-Otín, C., M. A. Blasco, L. Partridge, M. Serrano, and G. Kroemer. 2023. "Hallmarks of Aging: An Expanding Universe." *Cell* 186, no. 2: 243–278. <https://doi.org/10.1016/j.cell.2022.11.001>.
- Maldonado, E., S. Morales-Pison, F. Urbina, and A. Solari. 2023. "Aging Hallmarks and the Role of Oxidative Stress." *Antioxidants (Basel)* 12, no. 3: 651. <https://doi.org/10.3390/antiox12030651>.

- Meng, L., Y. Wei, Y. Liang, Q. Hu, and H. Xie. 2022. "Stem Cell Homing in Periodontal Tissue Regeneration [Review]." *Frontiers in Bioengineering and Biotechnology* 10: 1017613. <https://doi.org/10.3389/fbioe.2022.1017613>.
- Miller, R. A., Q. Chu, J. Xie, M. Foretz, B. Viollet, and M. J. Birnbaum. 2013. "Biguanides Suppress Hepatic Glucagon Signalling by Decreasing Production of Cyclic AMP." *Nature* 494, no. 7436: 256–260. <https://doi.org/10.1038/nature11808>.
- Moiseeva, O., X. Deschênes-Simard, E. St-Germain, et al. 2013. "Metformin Inhibits the Senescence-Associated Secretory Phenotype by Interfering With IKK/NF- κ B Activation." *Aging Cell* 12, no. 3: 489–498. <https://doi.org/10.1111/acer.12075>.
- Morris, G. M., R. Huey, W. Lindstrom, et al. 2009. "AutoDock4 and AutoDockTools4: Automated Docking With Selective Receptor Flexibility." *Journal of Computational Chemistry* 30, no. 16: 2785–2791. <https://doi.org/10.1002/jcc.21256>.
- National Pharmacopoeia, C. 2020. *Pharmacopoeia of the People's Republic of China*, 319–320. China Medical Science Press.
- Needleman, I., and D. R. Clark. 2023. "Aging and the Periodontium." In *Newman and Carranza's Clinical Periodontology and Implantology*, edited by M. G. Newman, P. R. Klokkevold, S. Elangovan, and Y. L. Kapila, 14th ed. Elsevier.
- Nguyen-Thi, T. D., B. H. Nguyen-Huynh, T. T. Vo-Hoang, and T. Nguyen-Thanh. 2023. "Stem Cell Therapies for Periodontal Tissue Regeneration: A Meta-Analysis of Clinical Trials." *J Oral Biol Craniofac Res* 13, no. 5: 589–597. <https://doi.org/10.1016/j.jobcr.2023.07.001>.
- Nousid, L., P. Kanavros, and A. Barbouti. 2023. "Oxidative Stress-Induced Cellular Senescence: Is Labile Iron the Connecting Link?" *Antioxidants (Basel)* 12, no. 6: 1250. <https://doi.org/10.3390/antiox12061250>.
- Nuñez, J., F. Vignoletti, R. G. Caffesse, and M. Sanz. 2019. "Cellular Therapy in Periodontal Regeneration." *Periodontology* 2000 79, no. 1: 107–116. <https://doi.org/10.1111/prd.12250>.
- O'Boyle, N. M., M. Banck, C. A. James, C. Morley, T. Vandermeersch, and G. R. Hutchison. 2011. "Open Babel: An Open Chemical Toolbox." *Journal of Cheminformatics* 3: 33. <https://doi.org/10.1186/1758-2946-3-33>.
- Ogata, H., S. Goto, K. Sato, W. Fujibuchi, H. Bono, and M. Kanehisa. 1999. "KEGG: Kyoto Encyclopedia of Genes and Genomes." *Nucleic Acids Research* 27, no. 1: 29–34. <https://doi.org/10.1093/nar/27.1.29>.
- Pan, C., J. Liu, H. Wang, J. Song, L. Tan, and H. Zhao. 2017. "Porphyromonas gingivalis Can Invade Periodontal Ligament Stem Cells." *BMC Microbiology* 17, no. 1: 38. <https://doi.org/10.1186/s12866-017-0950-5>.
- Pan, M., Y. Wu, C. Sun, H. Ma, X. Ye, and X. Li. 2024. "Polygonati Rhizoma: A Review on the Extraction, Purification, Structural Characterization, Biosynthesis of the Main Secondary Metabolites and Anti-Aging Effects." *Journal of Ethnopharmacology* 327: 118002. <https://doi.org/10.1016/j.jep.2024.118002>.
- Papapanou, P. N., M. Sanz, N. Buduneli, et al. 2018. "Periodontitis: Consensus Report of Workgroup 2 of the 2017 World Workshop on the Classification of Periodontal and Peri-Implant Diseases and Conditions." *Journal of Periodontology* 89, no. 1: S173–s182. <https://doi.org/10.1002/jper.17-0721>.
- Piñero, J., J. M. Ramírez-Anguita, J. Saüch-Pitarch, et al. 2020. "The DisGeNET Knowledge Platform for Disease Genomics: 2019 Update." *Nucleic Acids Research* 48, no. D1: D845–d855. <https://doi.org/10.1093/nar/gkz1021>.
- Polidori, M. C., and P. Mecocci. 2022. "Modeling the Dynamics of Energy Imbalance: The Free Radical Theory of Aging and Frailty Revisited." *Free Radical Biology & Medicine* 181: 235–240. <https://doi.org/10.1016/j.freeradbiomed.2022.02.009>.
- Rad, M. R., F. Atarbashi-Moghadam, P. Khodayari, and S. Sijanivandi. 2022. "Periodontal Ligament Stem Cell Isolation Protocol: A Systematic Review." *Current Stem Cell Research & Therapy* 17, no. 6: 537–563. <https://doi.org/10.2174/1574888x17666220128114825>.
- Rafikova, E., N. Nemirovich-Danchenko, A. Ogmen, et al. 2024. "Open Genes-a New Comprehensive Database of Human Genes Associated With Aging and Longevity." *Nucleic Acids Research* 52, no. D1: D950–d962. <https://doi.org/10.1093/nar/gkad712>.
- Rashid, Z. A., and S. K. Bardaweel. 2023. "Novel Matrix Metalloproteinase-9 (MMP-9) Inhibitors in Cancer Treatment." *International Journal of Molecular Sciences* 24, no. 15: 12133. <https://doi.org/10.3390/ijms241512133>.
- Ren, M., Y. Zhao, Z. He, et al. 2021. "Baicalein Inhibits Inflammatory Response and Promotes Osteogenic Activity in Periodontal Ligament Cells Challenged With Lipopolysaccharides." *BMC Complementary Medicine and Therapies* 21, no. 1: 43. <https://doi.org/10.1186/s12906-021-03213-5>.
- Richardson, L., S. G. Wilcockson, L. Guglielmi, and C. S. Hill. 2023. "Context-Dependent TGFbeta Family Signalling in Cell Fate Regulation." *Nature Reviews Molecular Cell Biology* 24, no. 12: 876–894. <https://doi.org/10.1038/s41580-023-00638-3>.
- Ru, J., P. Li, J. Wang, et al. 2014. "TCMSP: A Database of Systems Pharmacology for Drug Discovery From Herbal Medicines." *Journal of Cheminformatics* 6: 13. <https://doi.org/10.1186/1758-2946-6-13>.
- Sanz, M., D. Herrera, M. Kerschull, et al. 2020. "Treatment of Stage I-III Periodontitis-The EFP S3 Level Clinical Practice Guideline." *Journal of Clinical Periodontology* 47, no. 22: 4–60. <https://doi.org/10.1111/jcpe.13290>.
- Scarpello, J. H., and H. C. Howlett. 2008. "Metformin Therapy and Clinical Uses." *Diabetes & Vascular Disease Research* 5, no. 3: 157–167. <https://doi.org/10.3132/dvdr.2008.027>.
- Schlett, J. S., M. Mettang, A. Skaf, et al. 2023. "NF- κ B Is a Critical Mediator of Post-Mitotic Senescence in Oligodendrocytes and Subsequent White Matter Loss." *Molecular Neurodegeneration* 18, no. 1: 24. <https://doi.org/10.1186/s13024-023-00616-5>.
- Seo, B. M., M. Miura, S. Gronthos, et al. 2004. "Investigation of Multipotent Postnatal Stem Cells From Human Periodontal Ligament." *Lancet* 364, no. 9429: 149–155. [https://doi.org/10.1016/s0140-6736\(04\)16627-0](https://doi.org/10.1016/s0140-6736(04)16627-0).
- Shang, F., S. Liu, L. Ming, et al. 2017. "Human Umbilical Cord MSCs as New Cell Sources for Promoting Periodontal Regeneration in Inflammatory Periodontal Defect." *Theranostics* 7, no. 18: 4370–4382. <https://doi.org/10.7150/thno.19888>.
- Songkiatisak, P., S. M. T. Rahman, M. Aqdas, and M. H. Sung. 2022. "NF- κ B, a Culprit of Both Inflamm-Ageing and Declining Immunity?" *Immunity & Ageing* 19, no. 1: 20. <https://doi.org/10.1186/s12979-022-00277-w>.
- Stelzer, G., N. Rosen, I. Plaschkes, et al. 2016. "The GeneCards Suite: From Gene Data Mining to Disease Genome Sequence Analyses." *Current Protocols in Bioinformatics* 54: 1–31. <https://doi.org/10.1002/cpbi.5>.
- Szklarczyk, D., A. L. Gable, K. C. Nastou, et al. 2021. "The STRING Database in 2021: Customizable Protein-Protein Networks, and Functional Characterization of User-Uploaded Gene/Measurement Sets." *Nucleic Acids Research* 49, no. D1: D605–d612. <https://doi.org/10.1093/nar/gkaa1074>.
- Tacutu, R., D. Thornton, E. Johnson, et al. 2018. "Human Ageing Genomic Resources: New and Updated Databases." *Nucleic Acids Research* 46, no. D1: D1083–d1090. <https://doi.org/10.1093/nar/gkx1042>.
- Tak, P. P., and G. S. Firestein. 2001. "NF-kappaB: A Key Role in Inflammatory Diseases." *Journal of Clinical Investigation* 107, no. 1: 7–11. <https://doi.org/10.1172/JCI11830>.

- UniProtConsortium. 2021. "UniProt: The Universal Protein Knowledgebase in 2021." *Nucleic Acids Research* 49, no. D1: D480–d489. <https://doi.org/10.1093/nar/gkaa1100>.
- Wang, J., S. Wu, Z. Li, L. Liu, Y. Pang, and J. Wei. 2021. "Inhibition of Nuclear Factor Kappa B Inducing Kinase Suppresses Inflammatory Responses and the Symptoms of Chronic Periodontitis in a Mouse Model." *International Journal of Biochemistry & Cell Biology* 139: 106052. <https://doi.org/10.1016/j.biocel.2021.106052>.
- Wang, S., X. Shi, J. Li, et al. 2022. "A Small Molecule Selected From a DNA-Encoded Library of Natural Products That Binds to TNF- α and Attenuates Inflammation In Vivo." *Adv Sci (Weinh)* 9, no. 21: e2201258. <https://doi.org/10.1002/advs.202201258>.
- Wen, S., X. Zheng, W. Yin, et al. 2024. "Dental Stem Cell Dynamics in Periodontal Ligament Regeneration: From Mechanism to Application." *Stem Cell Res Ther* 15, no. 1: 389. <https://doi.org/10.1186/s13287-024-04003-9>.
- Wiley, C. D., and J. Campisi. 2021. "The Metabolic Roots of Senescence: Mechanisms and Opportunities for Intervention." *Nature Metabolism* 3, no. 10: 1290–1301. <https://doi.org/10.1038/s42255-021-00483-8>.
- Wishart, D. S., Y. D. Feunang, A. C. Guo, et al. 2018. "DrugBank 5.0: A Major Update to the DrugBank Database for 2018." *Nucleic Acids Research* 46, no. D1: 1074–1082. <https://doi.org/10.1093/nar/gkx1037>.
- Wu, Y., M. Liu, X. He, et al. 2024. "A Breakthrough in Periodontitis Treatment: Revealing the Pharmacodynamic Substances and Mechanisms of Kouqiangjie Formula." *Journal of Ethnopharmacology* 323: 117738. <https://doi.org/10.1016/j.jep.2024.117738>.
- Xenos, D., P. Mecocci, and V. Boccardi. 2022. "A Blast From the Past: To Tame Time With Metformin." *Mechanisms of Ageing and Development* 208: 111743. <https://doi.org/10.1016/j.mad.2022.111743>.
- Xu, H. Y., Y. Q. Zhang, Z. M. Liu, et al. 2019. "ETCM: An Encyclopaedia of Traditional Chinese Medicine." *Nucleic Acids Research* 47, no. D1: 976–982. <https://doi.org/10.1093/nar/gky987>.
- Ye, H., L. Ye, H. Kang, et al. 2011. "HIT: Linking Herbal Active Ingredients to Targets." *Nucleic Acids Research* 39: D1055–D1059. <https://doi.org/10.1093/nar/gkq1165>.
- Zelová, H., and J. Hošek. 2013. "TNF- α Signalling and Inflammation: Interactions Between Old Acquaintances." *Inflammation Research* 62, no. 7: 641–651. <https://doi.org/10.1007/s00011-013-0633-0>.
- Zhai, Q., Z. Dong, W. Wang, B. Li, and Y. Jin. 2019. "Dental stem cell and dental tissue regeneration." *Frontiers in Medicine* 13, no. 2: 152–159. <https://doi.org/10.1007/s11684-018-0628-x>.
- Zhang, L., M. Liu, W. Liu, et al. 2021. "Th17/IL-17 Induces Endothelial Cell Senescence via Activation of NF- κ B/p53/Rb Signaling Pathway." *Laboratory Investigation* 101, no. 11: 1418–1426. <https://doi.org/10.1038/s41374-021-00629-y>.
- Zhang, M., A. L. Kho, N. Anilkumar, et al. 2006. "Glycated Proteins Stimulate Reactive Oxygen Species Production in Cardiac Myocytes: Involvement of Nox2 (gp91phox)-Containing NADPH Oxidase." *Circulation* 113, no. 9: 1235–1243. <https://doi.org/10.1161/circulationaha.105.581397>.
- Zhang, Z. F., S. H. Fan, Y. L. Zheng, et al. 2009. "Purple Sweet Potato Color Attenuates Oxidative Stress and Inflammatory Response Induced by d-Galactose in Mouse Liver." *Food and Chemical Toxicology* 47, no. 2: 496–501. <https://doi.org/10.1016/j.fct.2008.12.005>.
- Zhao, L., C. Xu, W. Zhou, et al. 2023. "Polygonati Rhizoma With the Homology of Medicine and Food: A Review of Ethnopharmacology, Botany, Phytochemistry, Pharmacology and Applications." *Journal of Ethnopharmacology* 309: 116296. <https://doi.org/10.1016/j.jep.2023.116296>.
- Zheng, S. 2020. "Protective Effect of Polygonatum Sibiricum Polysaccharide on D-Galactose-Induced Aging Rats Model." *Scientific Reports* 10, no. 1: 2246. <https://doi.org/10.1038/s41598-020-59055-7>.
- Zhou, Y., Y. Zhang, X. Lian, et al. 2022. "Therapeutic Target Database Update 2022: Facilitating Drug Discovery With Enriched Comparative Data of Targeted Agents." *Nucleic Acids Research* 50, no. D1: D1398–d1407. <https://doi.org/10.1093/nar/gkab953>.
- Zhu, C., Y. Zhao, X. Wu, et al. 2020. "The Therapeutic Role of Baicalein in Combating Experimental Periodontitis With Diabetes via Nrf2 Antioxidant Signaling Pathway." *Journal of Periodontal Research* 55, no. 3: 381–391. <https://doi.org/10.1111/jre.12722>.